공학박사 학위논문

Performance Analysis and Enhancing Strategies for Unlicensed Band Cellular Communication System

비면허대역 셀룰라 통신의
성능 분석 및 성능 향상 기법 연구

2021년 2월

서울대학교 대학원

전기·정보공학부

이 재 홍

공학박사 학위논문

Performance Analysis and Enhancing Strategies for Unlicensed Band Cellular Communication System

비면허대역 셀룰라 통신의
성능 분석 및 성능 향상 기법 연구

2021년 2월

서울대학교 대학원

전기·정보공학부

이 재 홍

Performance Analysis and Enhancing Strategies for Unlicensed Band Cellular Communication System

지도 교수 박 세 웅

이 논문을 공학박사 학위논문으로 제출함

2021년 1월

서울대학교 대학원

전기·정보공학부

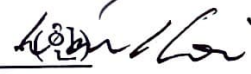이 재 홍

이재홍의 공학박사 학위 논문을 인준함

2020년 12월

위 원 장:	심 병 효	
부위원장:	박 세 웅	
위 원:	최 완	
위 원:	이 경 한	
위 원:	주 창 희	

Abstract

3GPP has developed 5 GHz unlicensed band LTE, referred to as licensed-assisted access (LAA). LAA adopts listen before talk (LBT) operation, resembling Wi-Fi's carrier sense multiple access with collision avoidance (CSMA/CA), to enable collision avoidance capability, while the frame structure overhead of each LAA downlink burst varies with the ending time of each preceding LBT operation.

In this dissertation, we propose numerical model to analyze unlicensed band cellular communication. Next, we consider the following two enhancements of unlicensed band cellular communication: (i) out-of-band emission (OOBE) aware additional carrier access, and (ii) Wi-Fi assisted hybrid automatic repeat request (H-ARQ) for unlicensed-band stand-alone cellular communication.

Given that, existing analytic models of Wi-Fi cannot be used to evaluate the performance of LAA, in this letter, we propose a novel Markov chain-based analytic model to analyze the performance of LAA network composed of multiple contending evolved NodeBs by considering the variation of the LAA frame structure overhead. LTE-LAA adopts adaptive modulation and coding (AMC) for the rate adaptation algorithm inherited from LTE. AMC helps the evolved nodeB (eNB) to select a modulation and coding scheme (MCS) for the next transmission using the channel quality indicator feedback of the current transmission. For the conventional LTE operating in the licensed band, there is no node contention problem and AMC performance has been well studied. However, in the case of LTE-LAA operating in the unlicensed band, AMC performance has not been properly addressed due to the collision problem. In this letter, we propose a novel Markov chain-based analysis model for analyzing LTE-LAA performance under a realistic channel model considering AMC operation. We adopt Rayleigh fading channel model widely used in wireless network analysis, and compare our analysis results with the results obtained from ns-3 simulator. Compari-

son results show an average accuracy of 99.5%, which demonstrates the accuracy of our analysis model.

Due to the requirement for a high data rate, the 3GPP has provided multi-carrier operation for LTE-LAA. However, multi-carrier operation is susceptible to OOBE and uses limited transmission power, resulting in inefficient channel usage. This paper proposes a novel multi-carrier access scheme to enhance channel efficiency. Our proposed scheme divides a transmission burst into multiple ones and uses short subframe transmission while meeting the transmission power limitation. In addition, we propose an energy detection algorithm to overcome the OOBE problem by deciding the channel status accurately. Our prototype using software-defined radio shows the feasibility and performance of the energy detection algorithm that determines the channel status with over 99% accuracy. Through ns-3 simulation, we confirm that the proposed multi-carrier access scheme achieves up to 59% and 21.5% performance gain in user-perceived throughput compared with the conventional LBT type A and type B, respectively.

Since the legacy LAA has deployment problem, 3GPP and MulteFire alliance proposed unlicensed band stand-alone cellular communication system. However, conventional unlicensed band stand-alone cellular communication system has low transmission probability of uplink control messages. This disertation proposes W-ARQ: Wi-Fi assisted HARQ which put uplink control messages into Wi-Fi block ACK frame. In addition we propose parallel HARQ and clustered Minstrel to enhance throughput performance of W-ARQ. Our proposed algorithm shows high throughput performance where conventional MulteFire shows almost zero throughput performance.

In summary, we analyze the performance of unlicensed-band cellular communication. By using the proposed model, we insist the legacy multi-carrier operation and H-ARQ of unlicensed cellular communication is not efficient. By this reason, we propose OOBE aware additional access and W-ARQ which achievee enhancements of network

performance such as UPT and throughput compared with state-of-the-art techniques.

Contents

List of Tables

List of Figures

Chapter 1

Introduction

1.1   Unlicensed Band Communication System

Nowadays, wireless communication technology has become an inexhaustible entity in our lives. It has evolved from the first generation, called analog wireless communication, to the second generation supporting short message service, the third generation supporting wireless Internet, and the fourth and fifth generations capable of multimedia communication. Until the third generation, most of the services were carried out in a licensed band, where business operators could use them at a financial price. However, from the fourth generation, which requires a high data rate, a wider frequency bandwidth is required. As a result, wireless communication technology has expanded the scope of application to a new resource, the unlicensed band, rather than the previously used licensed band.

Unlike the licensed band, the unlicensed band is a frequency band that anyone can use at no cost. Currently, there are 2.4 GHz, 5 GHz, and 60 GHz unlicensed bands used in wireless communication technology. Since the unlicensed band can be used by anyone, there are certain rules. There are rules for these unlicensed bands in each country, and the most referenced rules for communication technology development are those proposed by the European Telecommunication Standards Institute (ETSI) and the Fed-

eral Communications Commission (FCC). These protocols have rules to be followed by communication technologies operating in the unlicensed band, and the largest rule is the maximum transmission strength. Various communication devices exist in the unlicensed band. If there is no limit on the maximum transmission strength, signals are packed in all existing spaces, making communication impossible. Another important rule is listen-before-talk (LBT). In the unlicensed band, all communication devices used share a channel. Therefore, in order to share channels efficiently, transmission of other communication devices must be protected. For this role, each protocol stipulates that the unlicensed band communication technology always performs LBT operation.

As the importance of the unlicensed band communication technology has emerged, many unlicensed band communication technologies have emerged. Representatively, there is Wi-Fi that provides a high transmission rate. Wi-Fi started in 1997 with the IEEE 802.11 protocol providing a link speed of 2 Mbit/s, and has evolved to IEEE 802.11a, b, g, n, and ac. At the end of 2019, Wi-Fi alliance launched IEEE 802.11ax, dubbed Wi-Fi 6, and has been developing Wi-Fi technology that will continue to show better performance ever since. In the unlicensed band communication technology, Bluetooth and Zigbee do not provide high transmission rate, but support low power communication. Bluetooth was officially announced in 1999, and unlike Wi-Fi, which uses a 20 MHz bandwidth, it has a bandwidth of 1 MHz, and the recently developed Bluetooth 4.0 also communicates with low power using a 2 MHz bandwidth, which is a much narrower bandwidth than 20 MHz.

1.2 Overview of Existing Approaches

1.2.1 License-assisted access

In line with this trend, the 3GPP, which developed the third generation Wideband Code Division Multiple Access (WCDMA) and the fourth generation Long Term Evolution (LTE) technology and established the standard, proposed a method of using LTE tech-

nology in the unlicensed band. In March 2016, the 3GPP proposed License Assisted Access (LAA). LAA communicates using only the 5 GHz band, excluding the 2.4 GHz band, like IEEE 802.11ac. LAA uses the licensed band as an anchor to send and receive control signals in the licensed band, and in addition to the unlicensed band, donlink data is sent and received using carrier aggregation. Since LAA also uses unlicensed bands, it cannot escape from the regulation of unlicensed bands. The 3GPP proposed LBT operation in accordance with regulations for LAA communication technology. There are two LBTs of LAA: categry 2 and category 4. Category 4 LBT is similar to the existing Wi-Fi LBT operation. After the channel becomes idle, confirm that the channel is idle for the amount of time as long as the defer duration, and decrease the back-off counter value corresponding to the contention window size by one. When the back-off counter value becomes 0, the channel is occupied and data is transmitted, and collision can be avoided due to this back-off action. Category 2 LBT is similar to Wi-Fi's beacon frame transmission. If it is confirmed that the channel is idle for 25 us without performing a back-off operation, it is transmitted immediately. Category 2 LBT operation is used only in special cases, and this is typically the discovery reference signal transmission.

In the unlicensed band communication technology, there is a maximum transmission time that can be used once a channel is occupied, and this is called channel occupancy time. The channel occupancy time regulated by ETSI is generally 8 ms, and LAA follows it. Unlike Wi-Fi, LAA is an LTE-based technology, so frames must be transmitted according to the subframe boundary. However, the timing at which the LBT operation is performed cannot always coincide with the subframe boundary. Therefore, 3GPP proposed a new frame structure for LAA different from the existing LTE. First, after the LBT operation is finished, a reservation signal, which is a dummy signal in which data does not exist, is transmitted to occupy the channel to the subframe boundary. Reservation signal occupies the channel and prevents other devices from occupying the channel. If the LBT operation ends too early and there is too much

time remaining until the subframe boundary, the length of the reservation signal is lengthened and this causes a very large overhead. Therefore, 3GPP proposed an initial partial subframe with a length shorter than 1 ms in order to shorten the length of the reservation signal. The length of the initial partial subframe is 0.5 ms, so the length of the reservation signal cannot exceed 0.5 ms, thereby reducing the overhead. If LAA transmission ends at the subframe boundary, all of the maximum channel occupancy time may not be used. In this case, the time that the channel is empty becomes longer, which reduces overall network performance. Therefore, 3GPP proposed an ending partial subframe so that LAA transmission does not always end at the subframe boundary. This is a partial subframe with a length shorter than 1 ms and is located at the end of transmission. The 3GPP defines a total of 6 ending partial subframes each having a different length so that the maximum channel occupancy time can be used.

1.2.2 Further LAA

The 3GPP has continued to develop unlicensed band cellular communication technology even after LAA was proposed in release 13. In release 14 of 2017, an enhanced LAA (eLAA) was proposed that evolved LAA. LAA only supports downlink data transmission through the unlicensed band, but eLAA also enables uplink data transmission through the unlicensed band. Uplink data transmission has more restrictions than downlink data transmission. All uplink transmission should be transmitted using only the resources determined by the base station to the terminal. Therefore, eLAA additionally proposed an LBT operation for uplink. Also, since uplink transmission uses single carrier frequency division multiple access (SC-FDMA), unlike downlink using orthogonal frequency division multiple access (OFDMA), signaling different from the uplink signaling used in the existing LTE must be used. do. In the regulation of the unlicensed band, there is a rule that signals must exist in the entire frequency bandwidth to be used. Therefore, for this, 3GPP proposed an interlace structure in which the transmission signal is scattered along the frequency axis by changing the existing

SC-FDMA for eLAA.

After eLAA, 3GPP proposed a further enhanced LAA (feLAA) that further developed eLAA in release 15 of 2018. In the existing LAA and eLAA, only data transmission was possible through the unlicensed band, and control signal communication was performed through the licensed band. However, feLAA has extended this control signal communication to the unlicensed band. By allowing control signals to be transmitted in the unlicensed band, feLAA removes the restriction that the LAA should be connected to the licensed band eNB in an ideal backhaul. In eLAA, uplink transmission could only be performed on resources scheduled by the eNB. This is because the probability of LBT failure is so high that uplink transmission is virtually impossible. Therefore, feLAA attempted to solve this problem by proposing a grant-free uplink capable of uplink transmission even in resources other than those scheduled by the eNB.

With the advent of the 5G era, 3GPP has proposed new radio (NR), a 5G communication technology standard. In line with this, LAA, an unlicensed band communication technology based on LTE communication technology, has also changed to an NR-based unlicensed band communication technology. 3GPP named the NR-based unlicensed communication technology NR-ulicensed (NR-U) and applied the technology proposed by LAA to NR-U. In addition, NR-U proposed the mmWave communication technology in consideration of the 5G communication technology characteristics, and proposed a more diverse frame structure than the existing LAA for short latency. In addition, NR-U attempted to further increase the data rate by using the 5 GHz band used by the existing LAA and further up to the 6 GHz band. Currently, NR-U is being developed in release 16, and development is expected to be completed in release 17 in the future.

1.2.3 Non-3GPP Unlicensed Band Cellular Communication

Organizations other than 3GPP also proposed LTE-based unlicensed band cellular communication. MulteFire alliance proposed MulteFire that can operate independently in the unlicensed band without assistance from the licensed band. MulteFire has the advantage of having no restrictions on installation and strong security similar to Wi-Fi because it does not receive the help of licensed bands. MulteFire proposed a method for transmitting uplink data, transmitting downlink control signals, and transmitting uplink control signals to independently operate in an unlicensed band based on the LAA proposed by 3GPP. To this end, we independently developed a physical uplink contorl channel (PUCCH), which was not in the existing LAA, and proposed extended PUCCH (ePUCCH) and short PUCCH (sPUCCH). In addition, a physical random access channel (PRACH) and a PRACH procedure were also proposed to independently perform initial access in an unlicensed band.

1.3 Main Contribution

As the development of unlicensed band cellular communication technology is actively progressing, research on the unlicensed band cellular communication technology is also emerging. We analyzed the unlicensed band cellular communication technologies proposed by the 3GPP and non-3GPP organizations, and conducted research to improve the performance of these technologies.

1.3.1 Performance Analysis of LTE-LAA

We propose a Markov chain-based analytic model capable of analyzing LAA network performance considering the variation of LAA frame structure overhead. We also propose a Markov chain-based analysis model to analyze LTE-LAA network performance under a realistic Rayleigh fading channel.

The accuracy of the proposed analytic model was demonstrated by the compari-

son between analysis and simulation results. We also propose a Markov chain-based analysis model to analyze LTE-LAA network performance under a realistic Rayleigh fading channel. Our analysis model considers AMC adopted from LTE-LAA for the rate adaptation algorithm. We consider MCS selection of AMC under Rayleigh fading channel and how collisions affect AMC operation in LTE-LAA in terms of MCS selection and network throughput. We demonstrate our proposed model shows an average of 99.5% accuracy by comparing analysis and simulation results. Major contributions of this work are summarized as follows:

- We mathematically analyze the model of LTE-LAA considering the variation of LAA frame structure overhead.

- We propose a Markov chain-based analysis model to analyze AMC of LTE-LAA network performance under a realistic Rayleigh fading channel.

- Our proposed model shows an average of 99.5% accuracy by comparing analysis and simulation results.

1.3.2 Out-of-Band Emission Aware Additional Carrier Access for LTE-LAA Network

We present a novel multi-carrier access scheme for LTE-LAA that aims to reduce channel waste observed in the conventional multi-carrier operation. We also introduce the energy detection algorithm considering OOBE. Major contributions of this work are summarized as follows:

- We mathematically analyze the model of LTE-LAA multi-carrier operation and propose a new energy detection algorithm to overcome the problem of OOBE.

- Motivated by mathematical analysis, we measure OOBE on USRP-2943R and implement the energy detection algorithm considering OOBE on USRP-2943R to compare with the baseline energy detection scheme used in conventional communications.

- We propose an additional access scheme to enhance channel efficiency. Through extensive ns-3 simulations, we evaluate the proposed carrier access scheme and show its performance gain over the legacy schemes.

1.3.3   W-ARQ: Wi-Fi Assisted HARQ for Unlicensed Band Stand-Alone Cellular Communication System

We present HARQ operation for unlicensed band stand-alone cellular communication system. By this operation, unlicensed band stand-alone cellular communication system can transmits control messages using Wi-Fi block ACK. Since the control messages can be delivered, W-ARQ can successfully change the data rate and perform retransmission for failed transmissions. Major contributions of this work are summarized as follows:

- We propose novel HARQ operation for unlicensd band stand-alone cellular communication system.

- We propose parallel HARQ which support retransmission for W-ARQ.

- We propose clustered Minstrel rate adaptation to select data rate properly using W-ARQ.

1.4   Organization of the Dissertation

The rest of the dissertation is organized as follows.

Chapter 2 presents novel Markov analytic model to analyze the performance of LTE-LAA. First, we found that LTE-LAA transmission has Markov property by LBT operation and newly defined frame structure. Based on this, we proposed a novel Markov model to analyze the performance LTE-LAA under realistic channel model.

In Chapter 3, we propose new multi-carrier operation for LTE-LAA. First, we analyze the impact of out-of-band emission (OOBE) by using Markov model proposed

in chapter 2. Then, we measure the OOBE using conventional software defined network device USRP and propose new energy detection method which is not affected by OOBE. Lastly, we propose new multi-carrier operation by accessing additional carrier perfectly obeying regulation and standard.

Chapter 4 presents W-ARQ, Wi-Fi assisted HARQ for unlicensed band stand-alone cellular communication system. First we analyze the rare probability of uplink control signal transmission on unlicensed band stand-alone cellular communication system. Then we propose W-ARQ protocol. W-ARQ transmits Wi-Fi signal right after the end of LAA signal. Due to these operations, W-ARQ can send an uplink control message in a block ACK of Wi-Fi. We propose parallel HARQ procedure which enable retransmission of LAA frame in W-ARQ and clustered Minstrel rate adaptation algorithm which can change data rate properly.

Finally, Chapter 5 concludes the dissertation with the summary of contributions and discussion on the future work.

Chapter 2

Performance Analysis of LTE-LAA network

2.1 Introduction

Recently, 3GPP has developed 5 GHz unlicensed band LTE, referred to as *licensed-assisted access* (LAA), to cope with the increasing demand for network capacity since the licensed spectrum is scarce and costly. LAA utilizes supplemental downlink (DL) secondary component carrier (SCC) assisted by licensed primary component carrier (PCC) via carrier aggregation.

One important consideration for LAA is to ensure fair coexistence with the incumbent systems on 5 GHz unlicensed band such as Wi-Fi [1]. Accordingly, listen before talk (LBT) operation, similar to Wi-Fi's carrier sense multiple access with collision avoidance (CSMA/CA), is adopted by LAA to enable collision avoidance capability. It is worth noting that analyzing Wi-Fi network performance becomes feasible thanks to the well-known Markov chain-based analytic model, normally referred to as Bianchi model [2], which can characterize the behavior of CSMA/CA. However, LAA performance cannot be analyzed with the Bianchi model. The main reason is a new frame structure that has been introduced in LAA to accommodate flexible start and end of DL burst[1] caused by LBT operation, where the frame structure overhead encountered

---

[1]Throughout this section, we refer to the DL transmission within a number of consecutive subframes

in each DL burst is related to when the preceding LBT operation is completed. Such distinctive characteristics make it challenging to analyze LAA network performance.

There are several studies to analyze LAA network performance. In [3], LAA network capacity is analyzed using a semi-Markov chain model, where its effectiveness is validated by Monte-Carlo simulation. In [4–6], LAA and Wi-Fi coexistence performance is analyzed using stochastic geometry framework. However, these studies do not cope with the variation of the LAA frame structure overhead. Also, wireless channels fluctuate over time in the real world. A commonly accepted channel model is Rayleigh fading channel model. It is a statistical model, assuming that signals fade according to Rayleigh distribution. Several studies have analyzed the Rayleigh fading channel. Tan *et al* have analyzed the Rayleigh fading channel as a first-order Markov chain [7], and the authors in [8] have proposed a finite-state Markov model for the Rayleigh fading channel.

In this section, we propose a novel Markov chain-based analytic model to analyze LAA performance of AMC under Rayleigh fading channel, based on the finding that the frame structure overhead encountered in each DL burst depends only on the frame structure of previous DL burst and the backoff time in the preceding LBT operation, thus satisfying Markov property. We use the proposed model to calculate the expected LAA network throughput, which is compared with the results of the simulation. The difference between the analysis and the simulation results is merely 0.2% on average, thus demonstrating the accuracy of the proposed model.

2.2 Background

LAA supports only DL transmission by utilizing supplemental DL SCC. The LBT operation in LAA largely resembles enhanced distributed channel access (EDCA) of Wi-Fi [9]; LAA evolved NodeB (eNB) that intends to transmit first performs clear channel assessment (CCA) and starts DL burst after the channel has been sensed idle

---

as DL burst.

for a fixed time, d_{init}, and a random backoff time. The backoff time is determined as a CCA slot duration σ, which is defined as 9 μs,[2] multiplied by a random backoff counter bc, ranging from zero to contention window size (CWS). CWS is adjusted in a similar way to that in Wi-Fi ranging from CW_{min} to CW_{max}, i.e., binary exponential backoff. The values of d_{init}, CW_{min}, and CW_{max} are defined per *channel access priority class* [10]. The frame structure of LAA is mostly inherited from that of licensed band LTE except some disparities introduced to support flexible start and end of DL burst caused by LBT operation.

1) *Reservation signal*: If the starting point of a DL burst after random backoff is not aligned with subframe boundary, eNB can generate a *reservation signal* (RS), which is a dummy signal used to grab the channel, until the next upcoming subframe boundary. 2) *Maximum channel occupancy time*: A DL burst including reservation signal should not exceed *maximum channel occupancy time* (MCOT), which is defined per channel access priority class [10]. 3) *Initial and ending partial subframes*: In order to reduce reservation signal overhead, LAA introduces the concept of *initial partial subframe* (IPS) which allows LAA to start an actual data transmission at the center of a subframe. The existence of IPS depends on the starting point of a DL burst; a DL burst can start with IPS when the remaining time to the next subframe boundary is longer than 0.5 ms as illustrated in Fig. 2.1. Besides, depending on the starting point of a DL burst, the MCOT may not end at the end of a subframe. To utilize MCOT more efficiently, *ending partial subframe* (EPS) is also introduced to allow the last subframe of a DL burst to be utilized partially such that the MCOT can be exploited as much as possible. To adopt EPS with minimal specification efforts, the existing downlink pilot time slot (DwPTS) structure in time division duplexing (TDD) LTE is reused such that EPS can be one of the six types as summarized in Table 2.1 [10]. In particular, we refer to the case without EPS as EPS type 0. Fig. 2.1 illustrates LBT operation of LAA where a DL burst consists of RS, an IPS, several full subframes, and an EPS.

---

[2]The slot time in LAA is exactly the same as that in Wi-Fi.

Table 2.1: EPS type.

Type	0	1	2	3	4	5	6
Duration (μs)	0	214.583	428.646	643.229	714.583	785.938	857.292
# of symbols	0	3	6	9	10	11	12

The LBT operation is an important feature in LTE-LAA. It is very similar to enhanced distributed channel access in Wi-Fi. LTE-LAA eNB senses the channel first before transmission for a defer period that varies depends on the priority class. For example, if the traffic class is best effort, its defer period is 34 μs. Then, the eNB selects a random back-off counter value ranging from zero to its contention window size. It decreases the counter value by one when the channel is idle for the clear channel assessment (CCA) slot duration (9μs). When the back-off counter value reaches zero, the eNB transmits its signal immediately. Meanwhile, when the back-off counter values of multiple eNBs reach zero simultaneously, a collision occurs and their transmission fails.

The rate adaptation algorithm in LTE-LAA is inherited from that in the licensed band LTE, named AMC. The eNB transmits a reference signal every subframe. A user equipment (UE) receives a signal including the reference signal from the eNB, and calculates the received signal strength using the reference signal. Using the mapping table, the UE converts the calculated signal to interference plus noise ratio (SINR) of the received signal strength into a CQI value. In our model, we adopt the well-known mapping table proposed in [11], which shows the mapping os SINR estimates to MCS requiring 10% block error rate (BLER). Then, it transmits a CQI feedback message to the eNB. Upon receiving the CQI feedback message, the eNB selects an MCS for the next transmission according to the CQI value. Table 2.2 shows the mapping table between MCS, CQI, SINR, and modulation.

Table 2.2: Mapping table between MCS, CQI, SINR, and modulation

MCS	CQI	$SINR\ (dB)$	Modulation	MCS	CQI	$SINR\ (dB)$	Modulation
0	1	-6.7		16	9	10.3	16 QAM
2	2	-4.7		18	10	11.7	
4	3	-2.3	QPSK	20	11	14.1	
6	4	0.2		22	12	16.3	64 QAM
8	5	2.4		24	13	18.7	
10	6	4.3		26	14	21.0	
12	7	5.9	16 QAM	28	15	22.7	
14	8	8.1					

2.3 Proposed Markov-Chain Model

As with the previous efforts in wireless system analysis [2, 12, 13], in the proposed analytic model, we adopt 1) saturated traffic model where all the LAA eNBs always have packets to transmit, and 2) ideal channel where bit error rate (BER) is 0.

To analyze the network performance of LAA with saturated traffic model, we need to incorporate the system overhead by considering 1) the channel access overhead between two consecutive DL bursts, and 2) the frame structure overhead encountered during each DL burst. The channel access overhead can be easily incorporated by using Bianchi model, while for the frame structure overhead, we need a new model to cope with it. In this section, we first show that the variation of the frame structure overhead satisfies Markov property, and then elaborate our Markov chain-based analytic model, which is used to analyze the frame structure overhead.

2.3.1 Markov Property

For a DL burst, the frame structure overhead is determined by the duration of the RS (denoted as d_{rs}), that of the IPS (denoted as d_{ips}), and that of the EPS (denoted as d_{eps}). The duration of IPS is 500 μs if it exists; otherwise, 0 μs. When the traffic is saturated, to maximize channel occupancy time, eNB uses as many full subframes as possible such that the EPS type of the nth DL burst is determined as the longest EPS

Prev. EPS type and min. backoff time determine EPS type

0.5 ms

DL burst

Time

Prev. EPS type and min. backoff time determine the existence of IPS

IPS EPS Full Subframes RS d_{init}

↑ Subframe boundary   Min. backoff
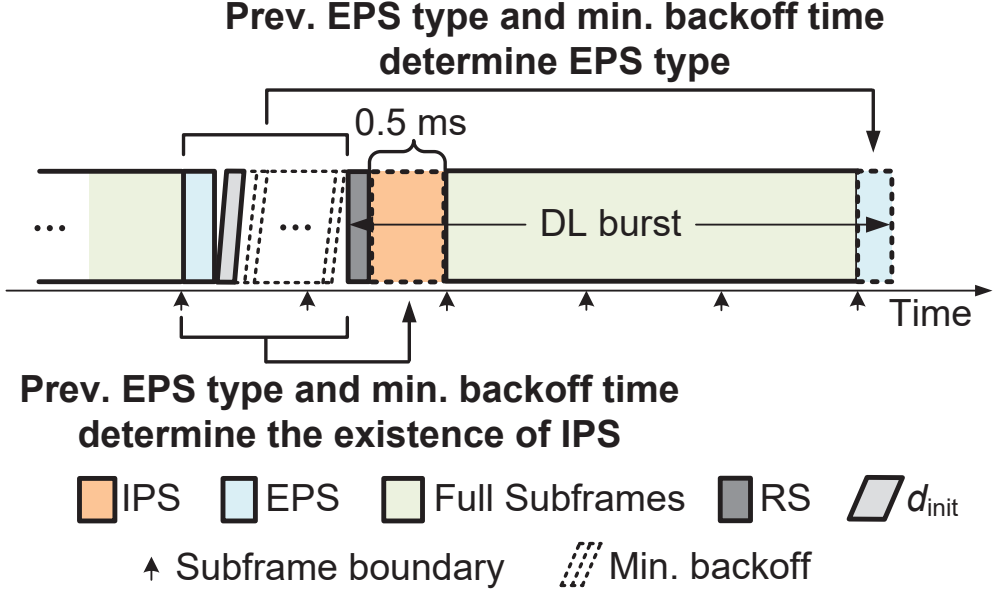
Figure 2.1: LBT operation of LAA.

(μs) satisfying

$$d_{\text{rs}}^{(n)} + d_{\text{ips}}^{(n)} + d_{\text{eps}}^{(n)} \leq 1000, \tag{2.1}$$

out of all the seven types, meaning that $d_{\text{eps}}^{(n)}$ is only dependent on $d_{\text{rs}}^{(n)}$ and $d_{\text{ips}}^{(n)}$, which are in turn dependent on the minimum backoff time, $bt_{\min}^{(n)}$, among those of all the contending eNBs, and the EPS duration of the $(n-1)$th DL burst, $d_{\text{eps}}^{(n-1)}$, due to the fact that

$$d_{\text{eps}}^{(n-1)} + d_{\text{init}}^{(p)} + bt_{\min}^{(n)} + d_{\text{rs}}^{(n)} + d_{\text{ips}}^{(n)} = \lambda \cdot 1000, \tag{2.2}$$

where $d_{\text{init}}^{(p)}$ indicates d_{init} for priority class p, and λ is a positive integer number at least one and possibly greater than one due mainly to the fact that $bt_{\min}^{(n)}$ can be much longer than 1000 μs. Note that the variation of the backoff time can be modelled as a Markov process as illustrated in [2]. Accordingly, if the EPS type of the $(n-1)$th DL burst is given, that of the nth DL burst is conditionally independent of that of other previous DL bursts, reflecting the Markov property as illustrated in Fig. 2.1.

15

2.3.2 Markov Chain Model for EPS Type Variation

In the proposed Markov chain, state s indicates the EPS type of a DL burst. The probability of state transition between the $(n-1)$th and the nth DL bursts is expressed as $\Pr\left(s_n = j | s_{n-1} = i\right)$, i.e., $d_{\text{eps}}^{(n-1)} = \text{eps}_i$ and $d_{\text{eps}}^{(n)} = \text{eps}_j$, where eps_i and eps_j represent the duration of type i and j EPS, respectively. Note that eps_j is determined as the longest EPS satisfying (2.1), such that

$$d_{\text{rs}}^{(n)} + d_{\text{ips}}^{(n)} + \text{eps}_j \leq 1000 < d_{\text{rs}}^{(n)} + d_{\text{ips}}^{(n)} + \text{eps}_{j+1}, \tag{2.3}$$

If we replace the sum of $d_{\text{rs}}^{(n)}$ and $d_{\text{ips}}^{(n)}$ with $1000 - \text{eps}_i + d_{\text{init}}^{(p)} + bt_{\text{min}}^{(n)}$ derived from (2.2), (2.3) is converted to

$$\left\lceil \frac{(\lambda - 1) \cdot 1000 + \text{eps}_j - \text{eps}_i - d_{\text{init}}^{(p)}}{\sigma} \right\rceil \leq bc_{\text{min}}^{(n)}$$
$$\leq \left\lceil \frac{(\lambda - 1) \cdot 1000 + \text{eps}_{j+1} - \text{eps}_i - d_{\text{init}}^{(p)}}{\sigma} - 1 \right\rceil, \tag{2.4}$$

where we indicate the minimum backoff counter value, $\frac{bt_{\text{min}}^{(n)}}{\sigma}$, as $bc_{\text{min}}^{(n)}$. From (2.4), we know that state transition is dependent only on the minimum backoff counter value, such that

$$\Pr\left(s_n = j | s_{n-1} = i\right) = \sum_{v \in \boldsymbol{I}_{i,j}} \Pr\left(bc_{\text{min}}^{(n)} = v\right), \tag{2.5}$$

where $i, j \in \{0, 1, ..., 6\}$, and $\boldsymbol{I}_{i,j}$ is the set of $bc_{min}^{(n)}$'s which lead to the transition from state i to j. $\boldsymbol{I}_{i,j}$ can be expressed as $\bigcup\limits_{\lambda=1}^{\lambda^{(p)}} \boldsymbol{I}_{i,j}^{(\lambda)}$, where

$$\boldsymbol{I}_{i,j}^{(\lambda)} = \boldsymbol{BC}^{(p)} \cap \boldsymbol{V}_{i,j}^{(p,\lambda)}. \tag{2.6}$$

Table 2.3: $\boldsymbol{I}_{i,j}$ leading to the state i to j transition for $p = 3$.

$i \backslash j$	0	1	2	3	4	5	6
0	[0,19]	[20,42]	[43,63]				
1		[0,19]	[20,42]	[43,50]	[51,58]	[59,63]	
2	[59,63]		[0,19]	[20,26]	[27,34]	[35,42]	[43,58]
3	[35,58]	[59,63]		[0,3]	[4,11]	[12,19]	[20,34]
4	[27,50]	[51,63]			[0,3]	[4,11]	[12,26]
5	[20,42]	[43,63]				[0,3]	[4,19]
6	[12,34]	[35,58]	[59,63]				[0,11]

Here, $\lambda^{(p)}$ is the maximum value of λ for priority class p, which is defined as

$$\lambda^{(p)} = \left\lceil \frac{CW_{\max}^{(p)} \cdot \sigma + d_{\text{init}}^{(p)} + \text{eps}_6}{1000} \right\rceil, \tag{2.7}$$

$\boldsymbol{BC}^{(p)}$ is a set of all possible backoff counter values, i.e., $[0, CW_{max}^{(p)}]$, for priority class p, and $\boldsymbol{V}_{i,j}^{(p,\lambda)}$ is a set including all the values of $bc_{min}^{(n)}$ satisfying (2.4) for priority class p and a specific λ. An example of $\boldsymbol{I}_{i,j}$ for priority class 3 is shown in Table 2.3.

Besides, to calculate the transition probability $\Pr(s_n = j | s_{n-1} = i)$, we need to know the distribution of $bc_{\min}^{(n)}$. Note that $bc_{\min}^{(n)} = v$ means that all the contending eNBs have backoff counter values no less than v and at least one eNB's backoff counter value is v, such that

$$\Pr\left(bc_{\min}^{(n)} = v\right) = \left(\sum_{l=v}^{CW_{\max}^{(p)}} q_l\right)^m - \left(\sum_{l=v+1}^{CW_{\max}^{(p)}} q_l\right)^m, \tag{2.8}$$

where q_l is the probability that an eNB has backoff counter value l, and m is the number of contending eNBs. q_l is obtained by utilizing Bianchi model [2]. For example, if the

priority class p is 3, we have

$$q_l = \begin{cases} b_{0,l} + b_{1,l} + b_{2,l}, & 0 \le l \le 15, \\ b_{1,l} + b_{2,l}, & 16 \le l \le 31, \\ b_{2,l}, & 32 \le l \le 63, \end{cases} \qquad (2.9)$$

where $b_{k,l}$ is the probability that an eNB has retransmission count k and the backoff counter value l when the Markov chain in Bianchi model is in steady state.

Finally, we construct the transition matrix $\mathbf{P}$ using (2.5) and (2.8), where ij-entry indicates $\Pr(s_n = j | s_{n-1} = i)$. The steady state distribution $\boldsymbol{\pi}$ can be obtained by solving

$$\boldsymbol{\pi}\mathbf{P} = \boldsymbol{\pi}, \qquad (2.10)$$

where the ith entry of $\boldsymbol{\pi}$ indicates the probability that EPS type of a DL burst is i in steady state.

2.3.3 LAA Network Throughput Estimation

As in the Bianchi model, we express the expected LAA network throughput in saturated traffic scenario as

$$\mathrm{E}\left[S\right] = \frac{P_s P_{tr} \mathrm{E}\left[B\right]}{(1 - P_{tr})\sigma + P_{tr}\mathrm{E}\left[T\right]}, \qquad (2.11)$$

where σ indicates the CCA slot duration, P_{tr} indicates the probability that at least one eNB transmits at a certain CCA slot, P_s indicates the probability that a transmitted DL burst succeeds without collision, $\mathrm{E}\left[B\right]$ indicates the expected amount of information bits delivered by a successful DL burst, and $\mathrm{E}\left[T\right]$ indicates the expected duration of a DL burst[3] added by $d_{\mathrm{init}}^{(p)}$. In (2.11), in order to calculate the expected LAA network

---

[3]Unlike Wi-Fi, the expected duration of a DL burst in LAA is not necessarily differentiated into two different terms to indicate successful and failed DL bursts, respectively, as in the Bianchi model, since the feedback for DL burst's reception status is transmitted via PCC, thus leading to the same duration of

throughput, we need to first calculate the expected duration of a DL burst, $\mathrm{E}\left[T\right]$, and the expected amount of information bits delivered by a successful DL burst, $\mathrm{E}\left[B\right]$.

First, for the calculation of $\mathrm{E}\left[T\right]$, recall that a DL burst normally consists of an RS, an IPS, a number of full subframes, and an EPS, where the portion of each component is determined by the minimum backoff counter value and the duration of the previous DL burst's EPS, which are assumed to be v and eps_i, respectively, in the following derivation. We first denote the time offset between the end of the backoff operation right before the DL burst and the next subframe boundary as $o\left(i, v\right)$, which is defined as

$$o\left(i, v\right) = 1000 - \left(\mathrm{eps}_i + d_{\mathrm{init}}^{(p)} + \sigma \cdot v\right) \bmod 1000. \tag{2.12}$$

In (2.12), modulo operation is entailed since the sum of eps_i, $d_{\mathrm{init}}^{(p)}$, and $\sigma \cdot v$ can be larger than 1000 μs, depending on the priority class. Then, there will be an IPS if $o\left(i, v\right)$ is larger than 500 μs such that

$$I_{\mathrm{ips}}(i, v) = \begin{cases} 1, & o\left(i, v\right) \geq 500, \\ 0, & o\left(i, v\right) < 500, \end{cases} \tag{2.13}$$

where I_{ips} is an indicator function, indicating the existence of IPS. Therefore, $d_{\mathrm{ips}}\left(i, v\right) = 500 I_{\mathrm{ips}}\left(i, v\right)$ (μs). Correspondingly, the duration of the RS becomes

$$d_{\mathrm{rs}}\left(i, v\right) = \begin{cases} o\left(i, v\right), & I_{\mathrm{ips}}\left(i, v\right) = 0, \\ o\left(i, v\right) - 500, & I_{\mathrm{ips}}\left(i, v\right) = 1. \end{cases} \tag{2.14}$$

Next, the number of full subframes $n_{\mathrm{full}}\left(i, v\right)$ is calculated as

$$n_{\mathrm{full}}\left(i, v\right) = \left\lfloor \frac{\mathrm{MCOT}^{(\mathrm{p})} - \left(d_{\mathrm{rs}}\left(i, v\right) + d_{\mathrm{ips}}\left(i, v\right)\right)}{1000} \right\rfloor, \tag{2.15}$$

and the duration of the EPS of current DL burst is determined as $\mathrm{eps}\left(i, v\right)$, which is

---

DL bursts in these two cases.

the longest EPS satisfying (2.1) given i and v. Therefore, the duration of the current DL burst is expressed as

$$T(i,v) = d_{\mathrm{rs}}(i,v) + d_{\mathrm{ips}}(i,v) + 1000 n_{\mathrm{full}}(i,v) + \mathrm{eps}(i,v), \qquad (2.16)$$

and $\mathrm{E}[T]$ becomes

$$E[T] = \left(\sum_{i=0}^{6} \sum_{v=0}^{CW_{\mathrm{max}}^{(p)}} \Pr(s=i) \Pr(bc_{\mathrm{min}} = v) T(i,v) \right) + d_{\mathrm{init}}^{(p)}. \qquad (2.17)$$

Similarly, when the previous DL burst's EPS type is i and the minimum backoff counter value is v, the number of information bits delivered by a DL burst is

$$B(i,v) = I_{\mathrm{ips}}(i,v) B_{\mathrm{ips}} + n_{\mathrm{full}}(i,v) B_{\mathrm{full}} + B_{\mathrm{eps}(i,v)}, \qquad (2.18)$$

where the amount of information bits in an IPS, B_{ips}, that in a full subframe, B_{full}, and that in an EPS with duration $\mathrm{eps}(i,v)$ are easily obtained by considering the LAA carrier bandwidth, the number of OFDM symbols per physical downlink control channel (PDCCH), and the modulation and coding scheme (MCS) index used by the DL burst, see [10]. Then, $\mathrm{E}[B]$ becomes

$$\mathrm{E}[B] = \sum_{i=0}^{6} \sum_{v=0}^{CW_{\mathrm{max}}^{(p)}} \Pr(s=i) \Pr(bc_{\mathrm{min}} = v) B(i,v). \qquad (2.19)$$

To analyze the AMC performance in LTE-LAA, we adopt Rayleigh fading channel, which is widely accepted in the literature. Thanks to previous efforts, we can include unlicensed band characteristics in the analytical Markov model for Rayleigh fading channel. As in the previous work, we assume that the channel does not change during one packet transmission. The probability density function (PDF) of Rayleigh

fading channel $f_r(\gamma)$ is given as

$$f_R(\gamma) = \frac{2\gamma}{\Omega}e^{-\frac{\gamma^2}{\Omega}}, \tag{2.20}$$

where γ is the received signal strength, and Ω is the average received signal strength. Fig. 2.2 illustrates the distribution of Rayleigh fading channel, where A_i for $i = 1, 2, \cdots, 15$, indicate the SINR thresholds for partitioning.

Through the SINR partitioning, we can model the Rayleigh fading channel as a one-dimensional Markov chain with state $s_i = \{A_i \leq r < A_{i+1}\}$, where r is the SINR of the received signal. Then we can obtain the state probability as

$$Pr(s_i) = \int_{A_i}^{A_{i+1}} f_R(\gamma)d\gamma. \tag{2.21}$$

Now we can express the state transition probability $\Theta_{i,j}$ from state s_i to state s_j as

$$\Theta_{i,j} = \begin{cases} \frac{N_{i+1}}{R_t Pr(s_i)}, & j = i+1, \\ \frac{N_i}{R_t Pr(s_i)}, & j = i-1, \\ 0, & \text{otherwise,} \end{cases} \tag{2.22}$$

where N_i is the level crossing rate of level A_i and R_t is the state transition rate.

We set A_i to the SINR value in Table 2.2 where i indicates the CQI value. Since the channel is continuous in the real world, state transitions occur only between neighboring states. We can express the level crossing rate N_i that represents how fast the channel fluctuates, as

$$N_i = \sqrt{\frac{2\pi A_i}{\Omega}}f_d e^{-\frac{A_i}{\Omega}}, \tag{2.23}$$

where f_d is the Doppler frequency term. Then we can calculate the state transition probability during the elapsed time D as

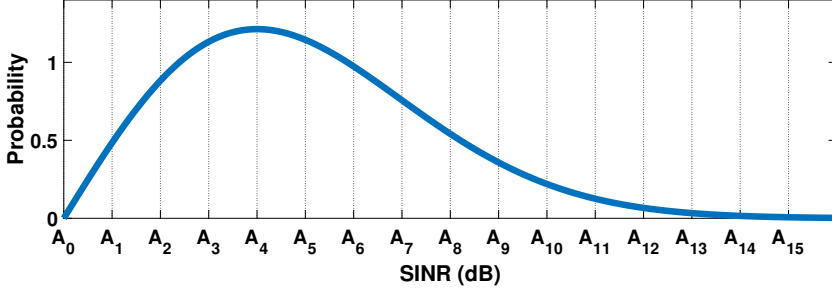$$Pr(s_j|s_i, D) = e_i\Theta^{E[D]R_t}, \tag{2.24}$$

Figure 2.2: Rayleigh distribution and SINR partitioning.

where $E[D]$ is the expected elapsed time and e_i is the basis vector of the i-th dimension in Cartesian coordinates.

By using these well-known equations to explain Rayleigh fading channel, we can easily calculate the state transition probability of Rayleigh fading channel under a LTE-LAA network system using AMC. Since the AMC for LTE-LAA chooses an MCS for the current transmission using the SINR of the previous transmission, we need to calculate the elapsed time between the start times of previous and current transmission for a single eNB. The elapsed time is the number of slots that exist between the previous and current transmission. Therefore we obtain the expected elapsed time by dividing the expected slot duration by the probability of a single eNB's transmission as

$$E[D] = \frac{(1 - p_{tr})\sigma + p_{tr}E[T]}{p_t}, \tag{2.25}$$

where p_{tr} is the probability that at least one eNB transmits in a slot which is given by

$$p_{tr} = 1 - (1 - p_t)^n, \tag{2.26}$$

where p_t is the probability that an eNB transmits in a slot, σ is the CCA slot length (9 μs), and $E[T]$ is the expected transmission time for an LTE-LAA packet, demonstrated in [14]. Since $E[T]$ is as long as the maximum channel occupancy time (MCOT) [14], it is much longer than σ. For a large number of nodes, p_t becomes small, then we can

22

approximate $E[D]$ to

$$E[D] = \frac{(1 - p_{tr})\sigma + p_{tr}E[T]}{p_t} \approx \frac{p_{tr}MCOT}{p_t} \approx n \times MCOT. \qquad (2.27)$$

Since $E[T]$ is a function of the error probability, we need to derive the error probability. Differently from an ideal channel, Rayleigh fading channel suffers not only collision errors but also channel errors due to changes in channel quality. Channel errors are caused by wrong MCS selection. Because the AMC in LTE-LAA selects an MCS for the current transmission using the previous channel quality, a channel error occurs when the current channel is worse than the previous one. Therefore we can express the channel error probability p_{ch-er} as

$$p_{ch-er} = p_t(1 - p_{col})p_d \sum_{j,i \in CQI} Pr(s_i)Pr(s_j|s_i, E[D]), \qquad (2.28)$$

where CQI is the set of CQIs with values ranging from 1 to 15 in LTE-LAA AMC and p_d is average decoding failure probability. There are many studies which show BLER curves [15, 16] using their own simulation environments. These results show that the BLER of a certain CQI converges to 0 at SINR where the BLER of the upper CQI is 10%. On the other hand, the BLER of a certain CQI is almost 1 at SINR where the BLER of the lower CQI is 10%. Therefore we set p_d to 1 for the $j < i$, and 0 for the $j > i$. For $i = j$, p_d is a function of SINR. Since we divide the SINR by section, we use the average decoding probability $E[p_d(i)]$ in the region of $A_i < SINR < A_{i+1}$ which can be obtained by the measured BLER curve. Then we can express the decoding

failure probability as [4] [5]

$$p_d = \begin{cases} 1, & j < i, \\ 0, & j > i, \\ E[p_d(i)], & j = i. \end{cases} \tag{2.29}$$

Note that p_{ch-er} includes the term $(1 - p_{col})$, where p_{col} indicates the collision probability.

In real situations, a collision does not always cause a transmission error. Even if a collision occurs, when the selected MCS is low enough to be tolerant of the low SINR caused by the collision, a data packet will be successfully transmitted. To analyze this, we formulate the collision probability under k interferers as

$$p_{col}^{(k)} = \binom{n-1}{k} p_t^k (1 - p_t)^{n-1-k}. \tag{2.30}$$

Now we derive the transmission error probability p_{err} when a collision occurs. For doing so, we define the current SINR value under k interferes when a collision occurs, as

$$S_{col}^{(k)} = \frac{R}{\sum_{l \in \mathcal{I}_k} I_l + N}, \tag{2.31}$$

where $\mathcal{I}_k$ is the set of k interferers, R is the received signal strength, I_l is the received interference signal strength from interferer l, and N is the noise floor. Combining (2.30) and (2.32), we can calculate the expected SINR value when a collision occurs as

$$S_{col} = \sum_{k=1}^{k=n-1} p_{col}^{(k)} S_{col}^{(k)}. \tag{2.32}$$

R and I follow Rayleigh distribution because they pass through the Rayleigh channel. Therefore, we can easily formulate the distribution of S_{col} using the summation and quotient of random variable properties. If $A_i \leq S_{col} < A_{i+1}$, a transmission error

---

[4]By partitioning the SINR threshold, p_d has more variable values but this increases the complexity of the model.

[5]We set p_d to 0.05 which is the median value between 10% and 0% BLER in our simulation.

occurs when the previous SINR is larger than A_{i+1}, which means the chosen MCS is not tolerant of S_{col}. We divide the collision error into two cases. First, a collision error occurs in the current transmission with no collision in the previous transmission. In this case, $i > j$ when the previous transmission SINR is in $A_i \leq S_{col} < A_{i+1}$, and the current SINR with collision is in $A_j \leq S_{col} < A_{j+1}$. Second, a collision error occurs in the current transmission with collision in the previous transmission. In this case, $i > j$ when the previous SINR with collision is in $A_i \leq S_{col} < A_{i+1}$, and the current SINR is in $A_j \leq S_{co} < A_{j+1}$. Normally, such a collision error occurs when the number of interferers for the current transmission with collision is larger than that for the previous transmission.

(a) CQI distribution with SNR = 10 dB, n=2

(b) CQI distribution with SNR = 15 dB, n=2

(c) CQI distribution with SNR = 20 dB, n=2

(d) CQI distribution with SNR = 10 dB, n=3

(e) CQI distribution with SNR = 15 dB, n=3

(f) CQI distribution with SNR = 20 dB, n=3

(g) CQI distribution with SNR = 10 dB, n=4

(h) CQI distribution with SNR = 15 dB, n=4
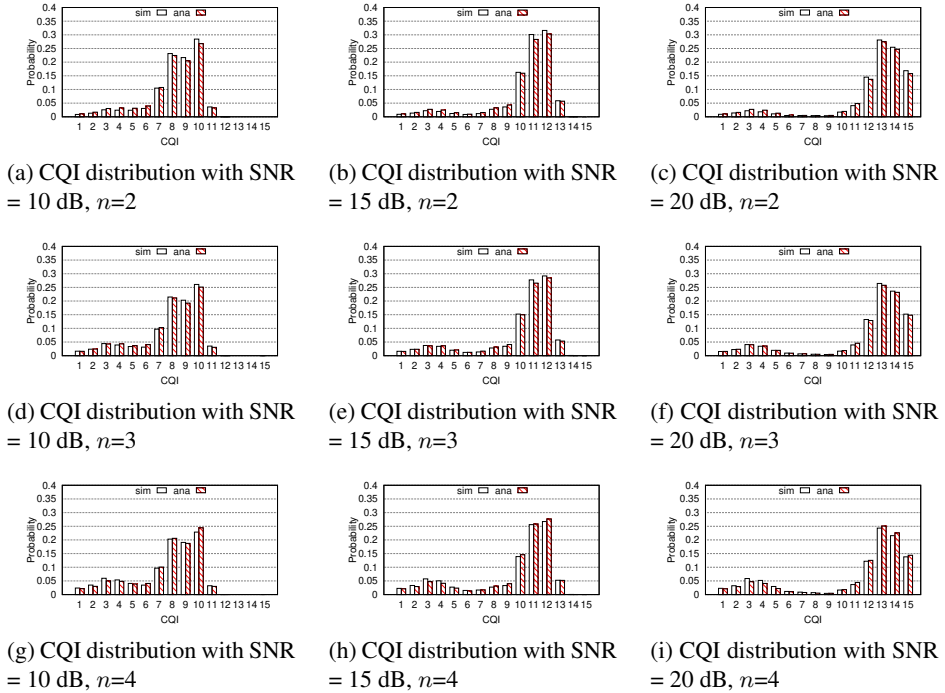
(i) CQI distribution with SNR = 20 dB, n=4

Figure 2.3: CQI distribution with MCOT = 2 ms.

Since the saturated traffic LTE-LAA system and Rayleigh channel model have the Markov property, in a stationary condition, S_{col} for each transmission has the same probability. Therefore, we can express the collision error probability as

$$p_{col-er} = (1 - p_{col}) \left(\sum_{\substack{j<i \\ j,i \in CQI}} Pr(S_{col}[T_{cur}] < A_j | s_i) \right)$$
$$+ p_{col} \left(\sum_{j \in CQI} Pr(S_{col}[T_{cur}] < A_j | A_j \leq S_{col}[T_{prev}]) \right), \tag{2.33}$$

where T_{cur} is the current transmission slot and T_{prev} is the previous transmission slot. From [2], we can express the collision probability as

$$p_{col} = \sum_k p_{col}^{(k)} = 1 - (1 - p_t)^{n-1}. \tag{2.34}$$

3GPP proposes hybrid automatic repeat request (HARQ) to combat the channel error. When a channel error occurs, eNB retransmits the failed packet and the UE combines the failed packet with the retransmitted one to increase decoding performance. In [17], the authors introduce the SNR gain SG which is modeled by the obtained BLER result from simulation. SG is the difference between the BLER curves of the retransmission and original transmission at the BLER of 10% for each CQI. We adopt this term to analyze the impact of HARQ on system performane of LTE-LAA. The required SINR A_i for MCS_i becomes the lower amount of SG_i due to HARQ. We set A_i' as $A_i - SG_i$.[6] Then the channel error probability of the retransmitted packet is expressed as

$$p_{ch-er}^{(ret)} = p_t(1 - p_{col})p_d \sum_{j,i \in CQI} Pr(s_i)Pr(s_j | s_i, E[D])p^{(ret)}(j,i), \tag{2.35}$$

where $p^{(ret)}(j,i)$ is

$$p^{(ret)}(j,i) = \begin{cases} \int_{A_j}^{A_i - SG_j} f_R(\gamma)d\gamma, & A_j \leq A_i - SG_j, \\ 0, & A_j > A_i - SG_j. \end{cases} \tag{2.36}$$

---

[6]we consider $RV = 1$ due to the lack of space. When RV is larger than one, SG is a function of RV and the probabilities have the terms of serial error probability.

The collision error probability of the retransmitted packet is expressed as

$$
\begin{aligned}
p_{col-er}^{(ret)} = (1 - p_{col}) & \left(\sum_{\substack{j<i \\ j,i \in CQI}} Pr(S_{col}/[T_{cur}] < A_j'|s_i) \right) \\
+ p_{col} & \left(\sum_{j \in CQI} Pr(S_{col}[T_{cur}] < A_j'|A_j \leq S_{col}[T_{prev}]) \right),
\end{aligned}
\tag{2.37}
$$

Indicating the probability of channel error and collision error of a non-retransmitted packet by superscript (n), we obtain the channel error probability and collision error probability considering HARQ as

$$
\begin{aligned}
p_{ch-er} &= (1 - p_{err})p_{ch-er}^{(n)} + p_{err}p_{ch-er}^{(ret)}, \\
p_{col-er} &= (1 - p_{err})p_{col-er}^{(n)} + p_{err}p_{col-er}^{(ret)}.
\end{aligned}
\tag{2.38}
$$

A transmission error occurs when either a channel or collision error occurs. Therefore we can calculate the transmission error probability p_{err} as

$$
p_{err} = 1 - (1 - p_{col-er})(1 - p_{ch-er}).
\tag{2.39}
$$

Then we can calculate the transmission probability of a single eNB p_t from [2] by replacing the collision probability with p_{err}, as

$$
p_t = \frac{2(1 - p_{err})}{(1 - 2p_{err})(W + 1) + p_{err}W(1 - (2p_{err})^m)},
\tag{2.40}
$$

where W is the maximum contention window size and m is the maximum back-off stage, and W and m are determined by the traffic class.

To analyze throughput performance, we need to calculate the expected MCS, $E[MCS]$, for each transmission [14].

The MCS distribution is the same as the distribution of CQI values determined by (2.21). However, if a collision occurs, the CQI distribution is a function of the
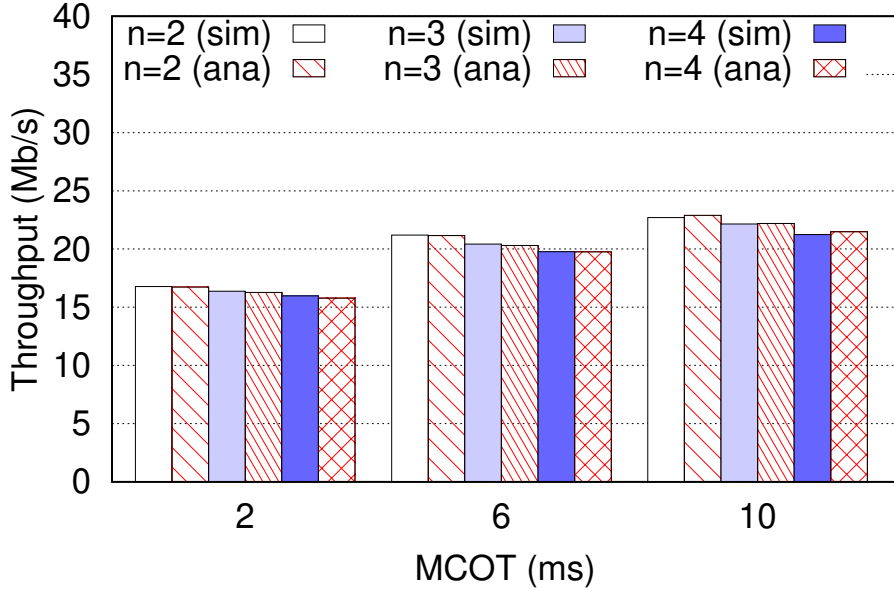
Figure 2.4: Throughput results with 10 dB SNR.

SINR value of the transmission with collision. Therefore, $E[MCS]$ is the sum of the distributions of each CQI value in collision and no-collision conditions. Since LTE-LAA transmits packet with transport block which is mapped into the certain MCS, to analyze throughput performance we calculate expected transport block size $E[TB]$ which can be expressed as,

$$
\begin{aligned}
E[TB] =& (1 - p_{col}) \left(\sum_{i \in CQI} Pr(s_i) TB_{MCS_i} \right) \\
&+ p_{col} \left(\sum_{i \in CQI} Pr(S_{col} \leq A_i) TB_{MCS_i} \right).
\end{aligned}
\tag{2.41}
$$

Since we assume non-ideal channels, the estimated throughput should take into account the error probability for each MCS. Since an error occurs when the channel quality for the current transmission is worse than that for the previous transmission, we can express the channel error probability for $MCS\ i$ as
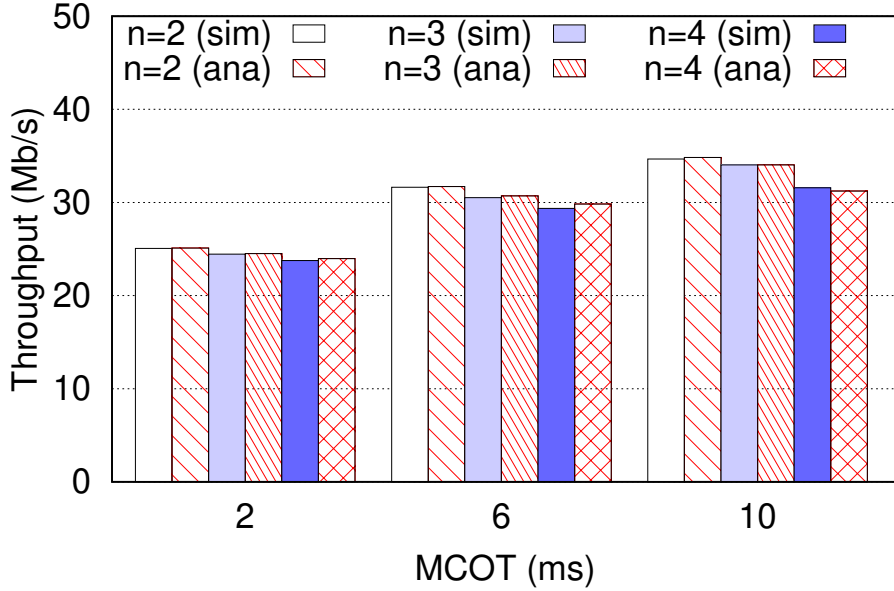
28

Figure 2.5: Throughput results with 15 dB SNR.

$$p_{ch-er}^{(i)} = (1 - p_{col})p_d \sum_{j \in CQI} Pr(s_i|s_j, E[D])$$
$$+ p_{col}Pr(S_{col} < A_i). \tag{2.42}$$

Combining (2.41), (2.42), and (2.33), we obtain $E[TB]$ under Rayleigh fading channel as

$$E[TB] = (1 - p_{col})\left(\sum_{i \in CQI} Pr(s_i)p_{ch-er}^{(i)}TB_{MCS_i}\right)$$
$$+ p_{col}p_{col-er}^{(i)}TB_{MCS_i}, \tag{2.43}$$

which directly helps us obtain the throughput of LTE-LAA by replacing the expected number of bits with $E[TB]$ in the throughput equation in [14].
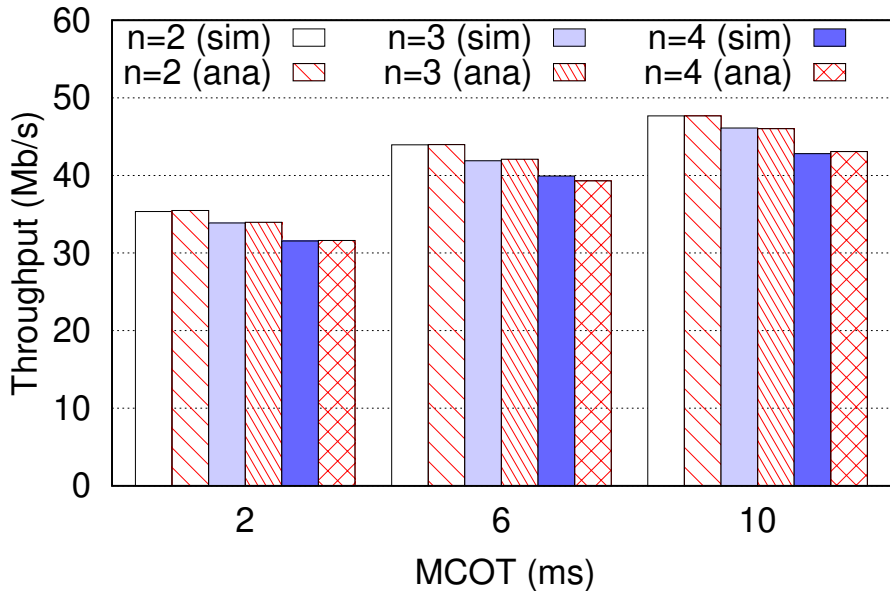
Figure 2.6: Throughput results with 20 dB SNR.

2.4 Model Validation

To validate the accuracy of the proposed analytic model, we compare the analysis results obtained using the proposed analytic model with simulation results in terms of the distribution of $bc_{\min}$, that of EPS type, and the expected LAA network throughput.

We implement an LAA simulator with MATLAB, and run the simulation for 300 iterations. In each iteration, there are 10^8 DL bursts transmitted by m contending eNBs fully saturated with DL traffic, where the starting point of the first DL burst is randomized to make the EPS type of the first DL burst evenly distributed. In the simulation, we make the wireless channel ideal such that a DL burst fails only if there is a collision. We assume all eNBs use the highest MCS, 20 MHz channel bandwidth, and priority class 3.

Fig. 2.7 shows the comparison between the analysis and the simulation results in terms of bc_{min} probability mass function (PMF). We observe that as the number of eNBs increases, the analysis and the simulation results become closer. Such tendency
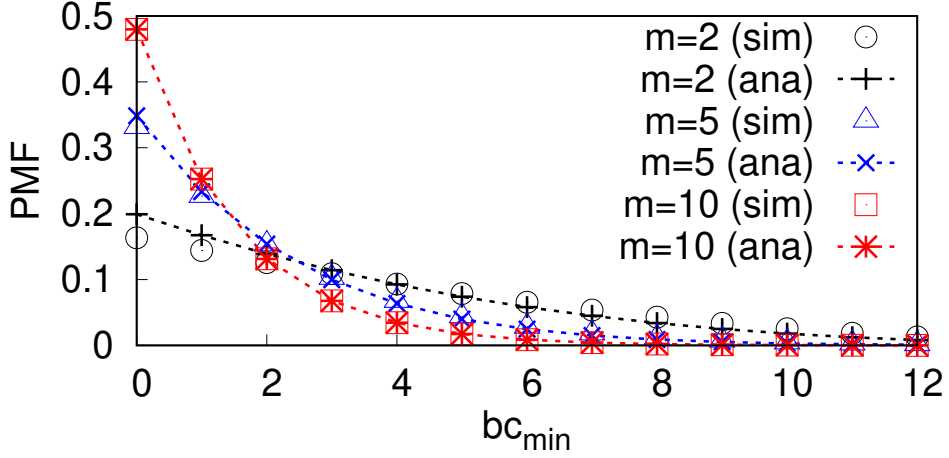
Figure 2.7: Model validation in terms of $bc_{\min}$ distribution with 2, 5, and 10 contending eNBs.

is due to the assumption made in Bianchi model [2] that the probability of a DL burst being successful is always constant, which is applicable only when the number of contending eNBs becomes sufficiently large. Note that when the number m of the contending eNBs increases, the PMF of $bc_{\min}$ is more densely concentrated near zero, since as the number of bc values increases, their minimum tends to become smaller.

Fig. 2.8 shows the comparison between the analysis and the simulation results in terms of the distribution of the EPS type of DL burst. We observe that as the number m of eNBs increases, the analysis and the simulation results become closer, and are almost the same if m is greater than two. Fig. 2.9 shows the comparison between the analysis and the simulation results in terms of the LAA network throughput as MCOT increases. We adopt 2, 6, and 10 ms MCOTs corresponding to the minimum MCOT, the maximum MCOT defined in [18], and the maximum MCOT defined in [10], respectively. We observe that as MCOT increases, the LAA network throughput increases, since the ratio of the system overhead, i.e., d_{init}, RS, and backoff time, and the wasted portion in the last subframe of each DL burst to the portion of each DL burst conveying information bits decreases. Note that the analysis results closely
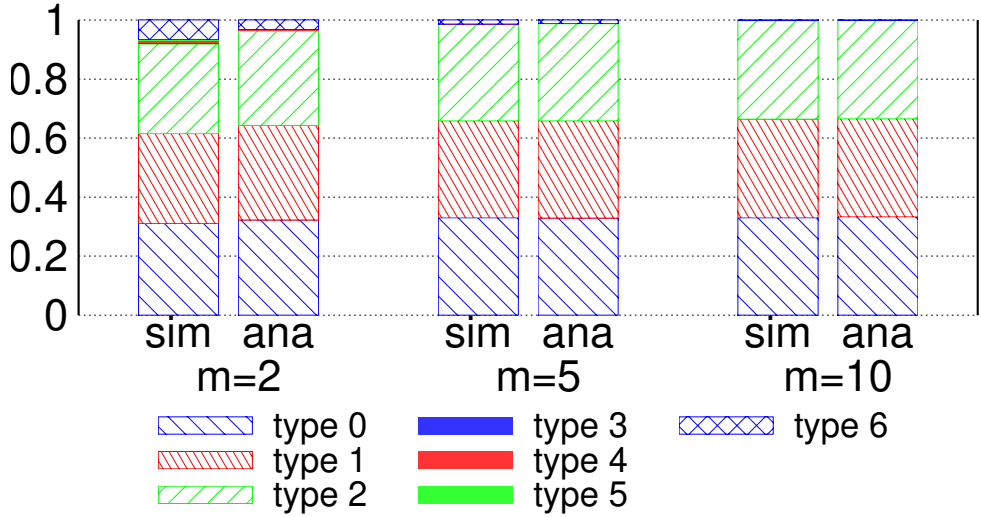
Figure 2.8: Model validation in terms of EPS type distribution with 2, 5, and 10 contending eNBs.

reflect the actual LAA performance such that the difference between the analysis and the simulation results is merely 0.2% on average.

To validate the accuracy of our analysis model, we compare analysis results with simulation results obtained from ns-3. Our validation has environment with 20 MHz transmission bandwidth, and full buffered traffic. Since we do not consider frequency selective channel, we assign one UE to each eNB with no mobility to concentrate the effect of Rayleigh fading channel. We vary the number of eNBs from two to four, and each simulation run time is 100 seconds. We set the MCOT to 2, 6, and 10 ms that are the minimum value, the maximum value specified in [19], and the maximum value specified in [10], respectively. Also we set the average signal to noise ratio (SNR) of the received signal to 10, 15, and 20 dB, respectively. Fig. 2.3 shows that the CQI distribution results from simulation and analysis when the MCOT is 2 ms. With the average received signal strength, the distribution of CQI bars moves to the right because the AMC selects a higher MCS. Observed CQI values below 6 are due to collision. As the number of contending eNBs increases from 2 to 4, the sum of distribution of CQI values below 6 increases from 0.09 to 0.16, which represents the increased collision
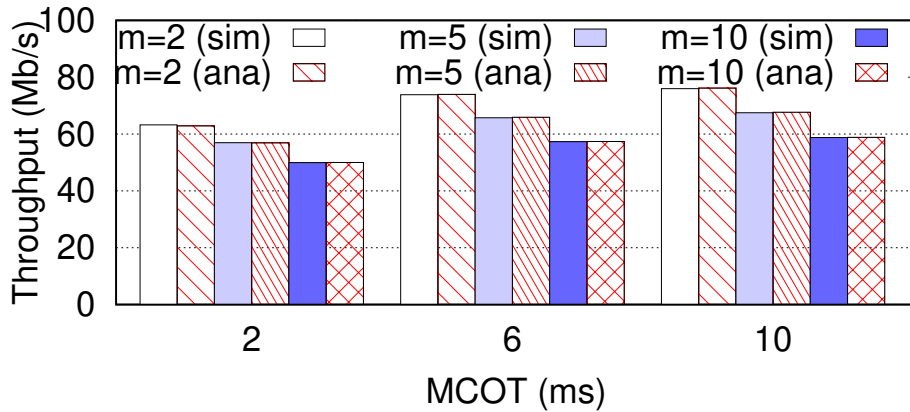
Figure 2.9: LAA network throughput evaluation.

probabilities.

Low MCSs are prevalent with the number of contending eNBs because the collision probability increases. The larger the number of interfering eNBs, the more widely distributed $SINR$ values can be. For CQI values below 6, our proposed model shows lower CQI distribution than ns-3 simulation. Such a tendency is due to the assumptions made in Bianchi model [2] where the collision probability is constant and there are sufficiently many contending eNBs.

The bars in Fig. **??** show throughput results calculated from our proposed model and obtained from ns-3 simulation. We observe that as the MCOT increases, LTE-LAA throughput increases since the overhead due to back-off, reservation signal and defer duration, decreases. On the other hand, network throughput decreases with the number of eNBs since the collision probability is proportional to the number of contending nodes. The network throughput increases with the SINR value. If the channel quality is good, the probability of choosing a higher MCS increases in the AMC operation. Although the number of contending eNBs is not large enough to meet the assumption of Bianchi's model, our analysis model shows a very low error rate of 0.5%. We expect that if the number of contending eNBs increases, our model becomes more accurate.

2.5 Summary

In this section, we proposed a Markov chain-based analytic model capable of analyzing LAA network performance considering the variation of LAA frame structure overhead. The accuracy of the proposed analytic model was demonstrated by the comparison between analysis and simulation results. Also, we proposed a Markov chain-based analysis model to analyze LTE-LAA network performance under a realistic Rayleigh fading channel. Our analysis model considers AMC adopted from LTE-LAA for the rate adaptation algorithm. We considered MCS selection of AMC under Rayleigh fading channel and how collisions affect AMC operation in LTE-LAA in terms of MCS selection and network throughput. We demonstrated our proposed model shows an average of 99.5% accuracy by comparing analysis and simulation results. LTE-LAA supports not only single-carrier operation but also multi-carrier operation, and LTE-eLAA supports uplink data transmission, so we also leave the analysis of multi-carrier operation of LTE-LAA, uplink transmission of LTE-eLAA, and frequency selective channel for future work.

Chapter 3

Out-of-Band Emission Aware Additional Carrier Access for LTE-LAA Network

3.1 Introduction

The 3rd-generation partnership project (3GPP) has greatly improved the quality of life of modern people by introducing long term evolution (LTE) as the demand for smart devices and multimedia applications increases exponentially. Nowadays, the paradigm of services we enjoy is changing with more diverse requirements and experiences. The 3GPP has introduced 5G new-radio (NR) to meet the requirements and explosive traffic demand. A key feature of NR is enhanced mobile broadband (eMBB), which requires a rate of gigabits/sec and medium latency [20].

To achieve eMBB, the 5G NR broadens its bandwidth using Millie-meter wave (mmWave) and unlicensed band. NR-U stands for NR that operates in unlicensed and licensed bands through carrier aggregation. Previous efforts have been made to operate LTE in unlicensed band, named license-assisted access (LAA), and NR-U is based on this. The 3GPP introduced LTE-LAA at first in release 13 to meet the growing traffic demand. Evolved node B (eNB) using LTE-LAA delivers critical information and guaranteed QoS services through the primary cell which uses the licensed band,

and it uses 5 GHz unlicensed band to opportunistically boost the data rate. LTE-LAA operations are similar to those of legacy LTE and include some additional features to work in unlicensed band. In the unlicensed band, channel efficiency is important because all existing devices share the same frequency band, and directly affects network performance.

LTE-LAA proposes a new frame structure i.e., frame structure type 3 to use the occupied channel efficiently. Because various communication technologies access the unlicensed band, LTE-LAA uses listen-before-talk (LBT) for their coexistence. For fair coexistence with IEEE 802.11 (i.e., Wi-Fi [9]), LTE-LAA complies with the LBT requirements in the European Telecommunications Standards Institute (ETSI) [19]. The use of multiple unlicensed band channels can boost the data rate, so LTE-LAA proposes to use multi-carrier operation. However, it does not properly consider physical aspects of the orthogonal frequency division multiplexing (OFDM) system, e.g., out-of-band emission (OOBE) and transmission power regulation in the unlicensed band.

In this paper, we introduce a novel multi-carrier operation for LTE-LAA and summarize our contributions as follows.

- We mathematically analyze the model of LTE-LAA multi-carrier operation and propose a new energy detection algorithm to overcome the problem of OOBE.

- Motivated by mathematical analysis, we measure OOBE on USRP-2943R and implement the energy detection algorithm considering OOBE on USRP-2943R to compare with the baseline energy detection scheme used in conventional communications.

- We propose an additional access scheme to enhance channel efficiency. Through extensive ns-3 simulations, we evaluate the proposed carrier access scheme and show its performance gain over the legacy schemes.

3.2 Related work and Background

3.2.1 Related work

LBT has been a major issue for LTE-LAA since LTE-LAA has been proposed. Many studies have shown the performance of LTE-LAA LBT using Markov model [6, 21–23]. These studies have analyzed the LBT of LTE-LAA and analyzed the coexistence of LTE-LAA with Wi-Fi. The authors in [24] have analyzed D2D communications considering the protocol for D2D transmission under the unlicensed band as LTE-LAA. In [14], the authors have analyzed LBT of LTE-LAA in more detail considering frame structure type 3. Many studies have proposed new LBT algorithms for LTE-LAA to overcome the fair coexistence problem in a single carrier. Choosing the optimal contention window size in LTE-LAA can be a solution for fair coexistence with Wi-Fi [25–27]. Some studies proposed asymmetry problem between CCA threshold and energy detection threshold [28, 29]. In [30–33], the authors proposed energy detection threshold adaptation algorithms for LBT to achieve fair coexistence of LTE-LAA and Wi-Fi.

There are several studies about the multi-carrier operation on LTE-LAA. In [34], the authors analyzed multi-carrier LBT operation for LTE-LAA and Wi-Fi using the Markov chain model based on [2] and noticed that that conventional multi-carrier operation is inefficient. Then they proposed a new multi-carrier LBT algorithm where the primary carrier controls sensing channel utilization of supplementary carriers. This algorithm contributed to increased total throughput, but there was no consideration of OOBE and various LBT types.

L. Vu *et al.* have studied the multi-carrier LBT mechanism for LTE-LAA [35]. This work shows that the general multi-carrier operation is infeasible due to OOBE. The authors have provided carrier grouping-based multi-carrier LBT that operates in types A and B by group. Although this work enhances system throughput under conventional LBT, room for better performance still exists as there are unoccupied carriers due to

OOBE.

Since OFDM has a significant OOBE problem, many studies have proposed OOBE reduction techniques. One of the most typical OOBE reduction techniques is guard band insertion, commonly used in practical OFDM systems such as Wi-Fi and LTE [9, 36].

Many studies have used time-domain windowing approaches to reduce the discontinuity of symbols, and the authors in [37, 38] proposed a signal overlaying using windowing. These approaches have reduced OOBE, but they are vulnerable to multi-path fading and have cyclic prefix overhead because they modify the cyclic prefix. Inserting cancellation subcarriers has been proposed in [39–41]. Cancellation subcarriers self-cancel the transmitter's side lobe that reduces OOBE. These studies significantly reduce OOBE at the receiver, but not enough at the transmitter.

3.2.2 Listen Before Talk

ETSI regulation [19] specifies two types of LBT operations: frame-based equipment (FBE) and load-based equipment (LBE). FBE is adopted by the LTE-unlicensed spectrum (LTE-U) proposed by LTE-U Forum. The LTE-U eNB that uses FBE LBT has periodic fixed frame periods for transmission, and it senses the channel to occupy for the fixed frame period only 9 μs before the fixed frame period. LBE LBT operation, similar to Wi-Fi's carrier sense multiple access with collision avoidance (CSMA/CA), is adopted by LTE-LAA to enable collision avoidance.

LTE-LAA eNB sets the contention window size to a random number between the minimum and maximum contention window values, i.e., a back-off counter value between zero and the selected contention window size. If the channel is idle for a period defined by priority class, the eNB decrements the back-off counter by one.[1] When the back-off counter reaches zero, then the eNB transmits a signal. Each transmission is within a single maximum channel occupancy time (MCOT), and the duration varies

---

[1]The length of the sensing slot is 9 μs in LTE-LAA.

by country. After the transmission ends, the eNB sets the contention window size to a new value according to the transmission result. For a successful transmission, the contention window size is set to the minimum value, otherwise, it is set to the doubled one.

3.2.3 Out-of-Band Emission

Conventional OFDM communication systems have serious OOBE problems. In typical OFDM systems, the frequency band is divided into multiple subcarriers. The transmitter transmits symbols on each subcarrier one by one. Because discontinuities occur at the boundary of symbols, the shape of power spectrum density on each carrier is a sinc function [42]. Although the side lobe of the sinc function crosses zero in adjacent subcarriers due to the orthogonal nature of subcarriers, the side lobe still exists in the out of frequency band. High OOBE causes interference to adjacent channels and degrades spectral efficiency. To mitigate performance degradation caused by OOBE, many standards and regulations limit the strength of OOBE that a device can emit.

3.3 Multi-carrier Operation of LTE-LAA

The 3GPP has standardized two types of multi-carrier operation: LBT type A and LBT type B [10, 43]. Each type has two subdivided types numbered 1 and 2. The alphabetic type distinguishes the access mechanism to multiple carriers, and the numbered type distinguishes the policy of selecting a back-off counter for each carrier.

LBT type A performs access on each carrier independently. After the eNB senses each carrier as idle for a defer duration, it decreases each carrier's back-off counter by one. If the back-off counter reaches zero on any carrier, the eNB transmits a signal on that carrier regardless of the condition of the other carriers.

LBT type B performs access to a randomly selected carrier among available carriers. The eNB senses whether the carrier is idle or busy during a defer duration in the
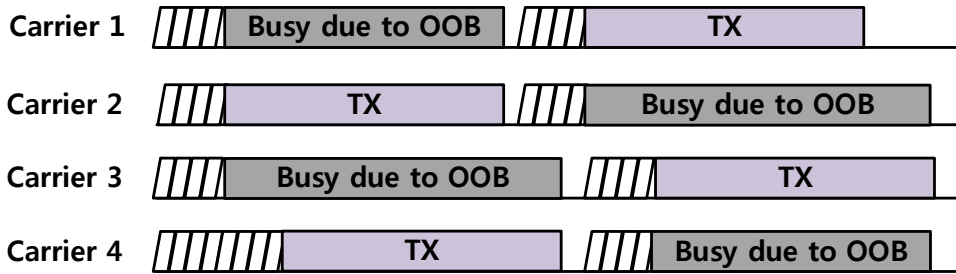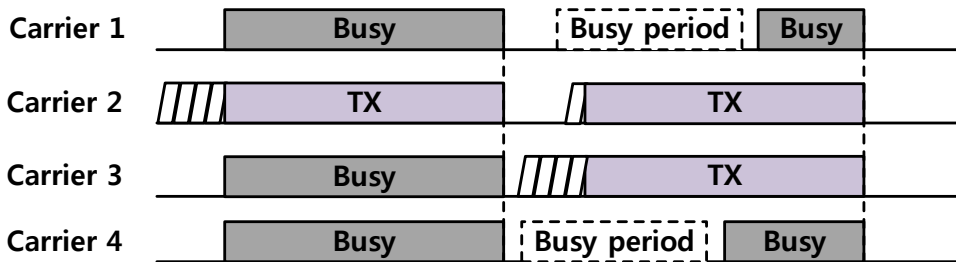
Figure 3.1: LBT type A.

Figure 3.2: LBT type B.

selected carrier. If the carrier is idle, the eNB decreases the back-off counter. When the back-off counter value reaches zero, the eNB checks if the other carriers are idle for 25 μs before the back-off counter value becomes zero. If the eNB determines any other carrier as idle, it occupies not only the selected carrier but also the other idle carrier. The operations of LBT type A and B are illustrated in Fig. **??**.

LBT type A allows independent access to each carrier, which should be idle when the eNB tries to access it. However, if the eNB has already occupied one carrier, other adjacent carriers that the eNB wants to access additionally may be affected by the OOBE of the occupied carrier [35]. In Fig. **??**(a), each of four carriers has its own back-off counter value. Since carrier 2 has the lowest back-off counter value, the eNB occupies the carrier 2 first. Although carriers 1 and 3 are idle, the eNB cannot decrement their back-off counter values due to the OOBE from carrier 2.
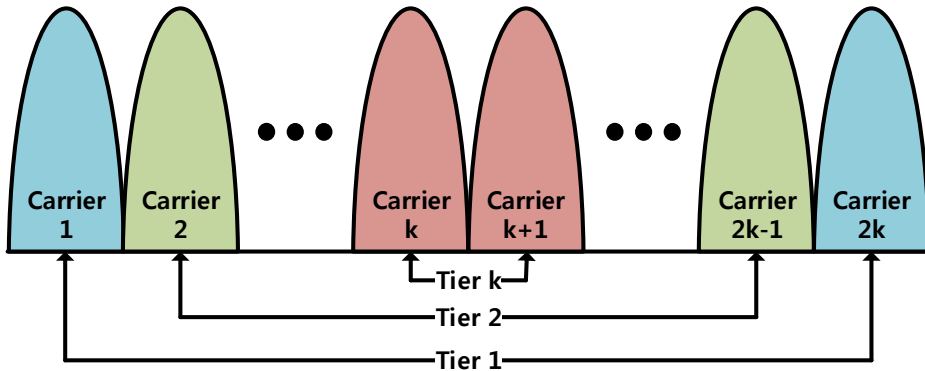
Figure 3.3: The number of carriers is even.

Carrier 4 which is not affected by the OOBE from carrier 2 is occupied by the eNB when its counter value becomes zero. When carrier 2 ends its transmission, carrier 1 decreases its back-off counter value after a defer duration while carrier 3 does not do so. This is because the OOBE from carrier 4 affects carrier 3. When the back-off counter value of carrier 1 becomes zero, the eNB transmits a signal on carrier 1, but in this turn, carrier 2 cannot decrease its back-off counter value due to the OOBE from carrier 1. Carrier 1 does not affect carriers 3 and 4, but carriers 3 and 4 will affect each other if either one transmits a signal since they are adjacent, resulting in inefficient channel use.

To numerically show the performance degradation due to the OOBE, we present a mathematical analysis model and analyze the performance of LBT type A. For OOBE analysis, we define the carrier tier according to the location of each carrier. Fig. **??** shows the tier of each carrier when the number of carriers is even or odd. Because the shape of OOBE is symmetric around the center frequency, carriers with the same tier are affected by the same OOBE.

Thanks to [2] and [14], we can analyze the performance of LTE-LAA network using the finite state Markov chain model. They define the state of the Markov chain as the set of the backoff stage value and the backoff counter value of the transmit-
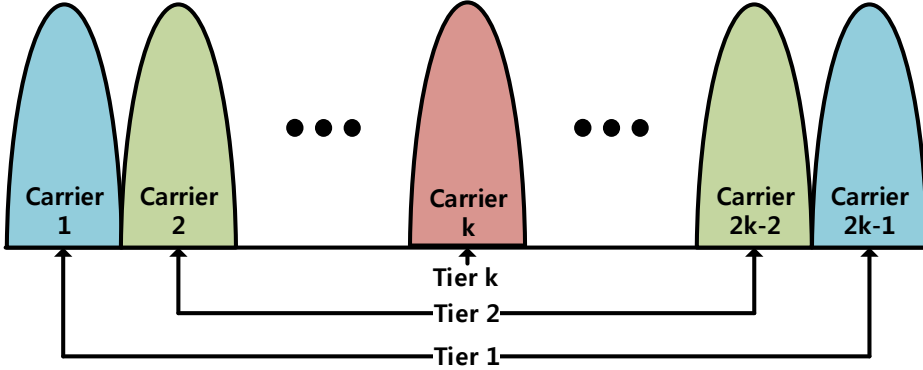
Figure 3.4: The number of carriers is odd.

ter, denoted by (l, m). Since there is no consideration about OOBE in these studies, the transition probability from (l, m) to $(l, m - 1)$ is always one. However, in our model, the transition probability is not one because each transmitter cannot decrease its backoff counter while the OOBE from adjacent carriers exists. Due to OOBE, the transmission probability on each carrier is different although the eNB using LBT type A performs LBT independently on each carrier. Therefore, the transition probability q is the probability that both adjacent carriers do not transmit packets. A carrier of tier k has two adjacent carriers with tiers $k - 1$ and $k + 1$, respectively. The transition probability of tier k carrier is affected by the transmission probability of tier $k - 1$ carrier and tier $k + 1$ carrier, expressed as τ_{k-1} and τ_{k+1}, respectively, such that

$$q_k = (1 - \tau_{k-1})(1 - \tau_{k+1}). \tag{3.1}$$

For $k = 1$, there is only one adjacent carrier whose tier is 2. Therefore

$$q_1 = (1 - \tau_2). \tag{3.2}$$

According to whether the number of carriers is odd or even (see Fig. **??**) , we can
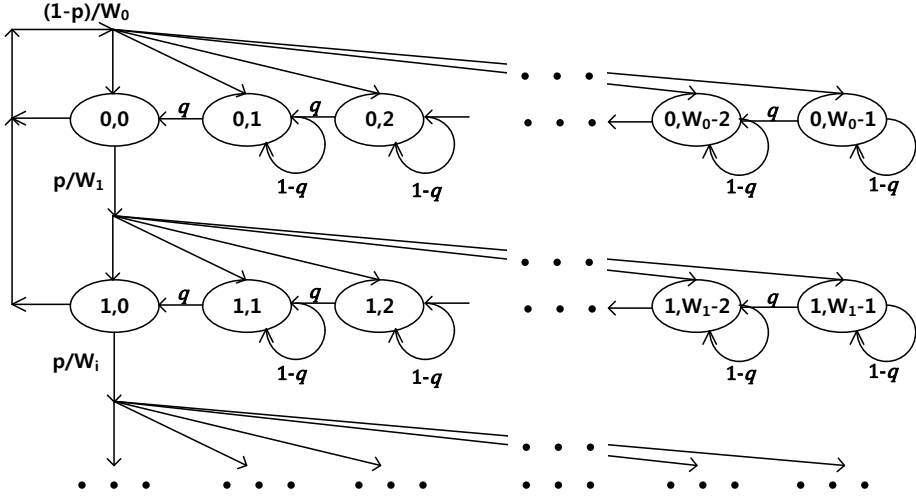
Figure 3.5: Proposed Markov model of multi-carrier operation considering OOBE.

similarly obtain the transition probability of the maximum tier carrier as

$$
q_{k_{max}} = \begin{cases} (1 - \tau_{(k_{max}-1)})(1 - \tau_{(k_{max}-1)}), & \text{odd}, \\ (1 - \tau_{(k_{max}-1)})(1 - \tau_{(k_{max})}), & \text{even}. \end{cases} \tag{3.3}
$$

Fig. 3.5 illustrates our proposed analysis model. Referring to [14], we can calculate the throughput performance of LTE-LAA $E[S]$ as

$$
E[S] = \frac{P_S P_{tr} E[B]}{(1 - P_{tr})\sigma + P_{tr} E[\text{COT}]}, \tag{3.4}
$$

where P_S is the probability of successful transmission, P_{tr} is the probability of at least one eNB transmits, and $E[B]$ is the expected size of data packets. The denominator represents the average slot time, and σ is the back-off slot time duration, i.e., 9 μs, and $E[COT]$ is the expected channel occupancy time. The average slot time in the OOBE existing environment is different from the non-OOBE environment. If there exists OOBE from adjacent carriers, the idle time of a device is the minimum back-

43

off time of the other devices, bc_{min}, because the slot gets busy after bc_{min} due to transmission from other devices.[2] Therefore we obtain the throughput performance of carrier tier k in OOBE existing environments as

$$E[S(k)] = \frac{P_S P_{tr} E[B]}{(1 - P_{tr})E[T_{\mathrm{idle}}] + P_{tr}E[\mathrm{COT}]}, \tag{3.5}$$

where the expected idle slot duration $E[T_{\mathrm{idle}}]$ is

$$E[T_{idle}] = \begin{cases} (1 - ((1 - \tau_{k-1})(1 - \tau_{k+1}))E[\mathrm{COT}] \\ +(1 - \tau_{k-1})(1 - \tau_{k+1})\sigma, & n = 1, \\ (1 - ((1 - \tau_{k-1})(1 - \tau_{k+1}))bc_{\mathrm{min}} \\ +(1 - \tau_{k-1})(1 - \tau_{k+1})\sigma, & n > 1. \end{cases} \tag{3.6}$$

OOBE is not an important issue in a saturated traffic environment because the empty channel created by OOBE will be filled with transmission from other devices. However, it degrades performance a lot in an unsaturated environment which we are considering. To analyze LTE-LAA in the unsaturated environment, we assume Poisson packet arrivals and active contending nodes introduced in [44]. For the packet arrival rate λ [packets/slottime] and service time $E[T]$, P_0 is computed as

$$P_0 = 1 - \frac{\lambda}{\mu}, \tag{3.7}$$

where μ is the average service rate equal to $1/E[T]$. Since the number of active nodes in the unsaturated traffic environment varies, we can estimate the distribution of the number of active contending nodes i among all the contending nodes N using P_0 as

$$\beta_i = \binom{N}{i}(1 - P_0)^i P_0^{(N-i)}. \tag{3.8}$$

---

[2]bc_{min} is easily obtained from [14].

Using the obtained distribution of active contending nodes, we have the throughput performance in the unsaturated traffic environment of carrier tier k as

$$E[S_{unsat}(k)] = \sum_{i=1}^{N} \beta_i E[S_i(k)].$$ (3.9)

Since the throughput matches the source rate in the unsaturated situation, throughput is not a meaningful performance metric. We use user perceived throughput (UPT) as a performance metric in the unsaturated situation, which is defined as the total file size divided by the time required to download the whole file per user. UPT can be calculated by dividing the throughput by the number of active contending nodes and normalizing it to a non-zero contending node probability such that,

$$E[U_{unsat}(k)] = \frac{\sum_{i=1}^{N} \beta_i E[S_i(k)]/i}{(1 - \beta_0)}.$$ (3.10)

We simulate the unsaturated traffic model with varying the number of contending eNBs, the number of carriers, and the packet arrival rate. Our proposed model shows the average accuracy of 96.4%. Fig. **??** shows the UPT performance of LTE-LAA obtained by MATLAB simulation and our proposed model. For low λ, UPT performance in the OOBE existing environment is low compared with that in the non-OOBE environment. For high λ and N, the performance gap between OOBE and non-OOBE environments becomes small. This is because the effect of OOBE is negligible in saturated environments due to the transmission of other devices. With the number of carriers, the performance gap between OOBE and non-OOBE environments increases. These confirm that LBT type A does not perform efficiently.

Let's go back to LBT type B that allows access of multiple carriers at the same time. LBT type B does not allow the eNB to occupy some carriers even when they are idle. Fig. **??**(b) shows an example where carrier 2 is chosen for access first. If the other carriers are busy when the back-off counter of carrier 2 becomes zero, the eNB only occupies carrier 2 and transmits a signal. After the end of transmission on carrier 2,
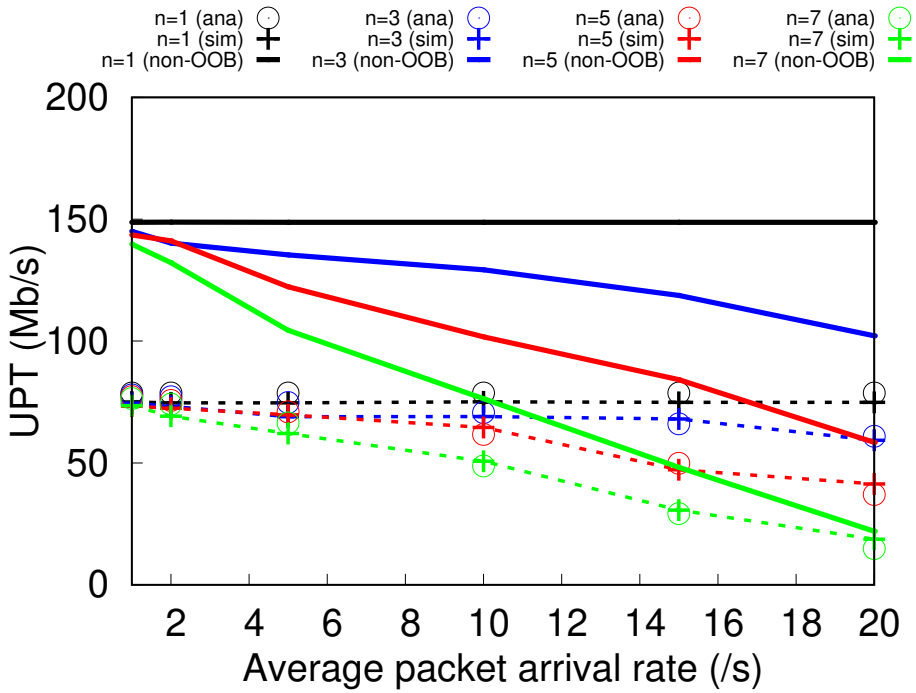
Figure 3.6: UPT performance analysis using the proposed Markov model in an OOBE environment in 2 carriers.

the eNB selects carrier 3 for access. Carrier 2 is idle when the back-off counter of carrier 3 reaches zero, while carriers 1 and 4 are not. Then, the eNB transmits signals on carriers 2 and 3. Although the busy period[3] ends on carriers 1 and 4 before the transmissions on carriers 2 and 3 are over, the eNB does not access carriers 1 and 4. This is because carriers 1 and 4 are considered busy until the transmissions on carriers 2 and 3 end, resulting in inefficient channel use. This motivates us to develop a new multi-carrier operation scheme next.

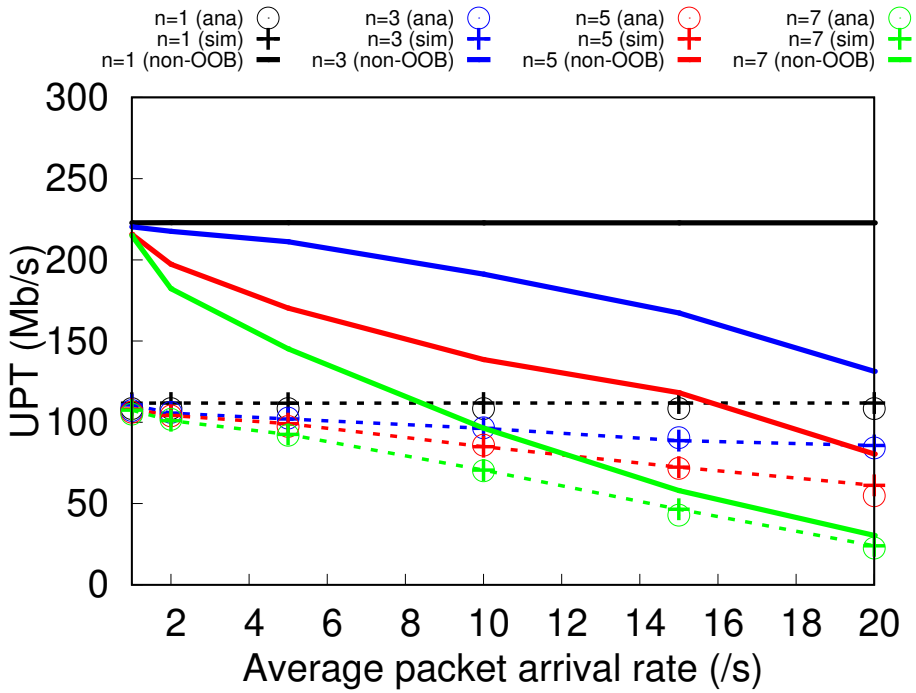[3]In this paper, we use the term busy period for a non-own signal.

Figure 3.7: UPT performance analysis using the proposed Markov model in an OOBE environment in 3 carriers.

3.4 Carrier Sensing considering Out-of-Band Emission

In OFDM communication systems, OOBE occurs due to non-contiguous symbols, and LTE-LAA is no exception to this.[4] Due to the close distance between radio-frequency modules using different carriers at the eNB, OOBE by own signal causes a serious problem to the transmitter. If an additionally accessible carrier (AAC) is located near an already occupied carrier (AOC), OOBE from the AOC causes the eNB to determine that the AAC is busy. This is because the OOBE level is higher than the CCA threshold until transmission on the AOC ends, even though the AAC is idle. The wrong decision caused by OOBE makes the eNB unable to access the AAC. To avoid OOBE, the eNB should transmit only on carriers that are not adjacent to each other. This approach

---

[4]The 3GPP limits the OOBE level of LTE-LAA to -52 dB of the transmission power, which can be -29 dBm when the eNB transmits signals with 23 dBm in [45]. Meanwhile, ETSI limits the OOBE level in [19] to -40 dB of the transmission power.
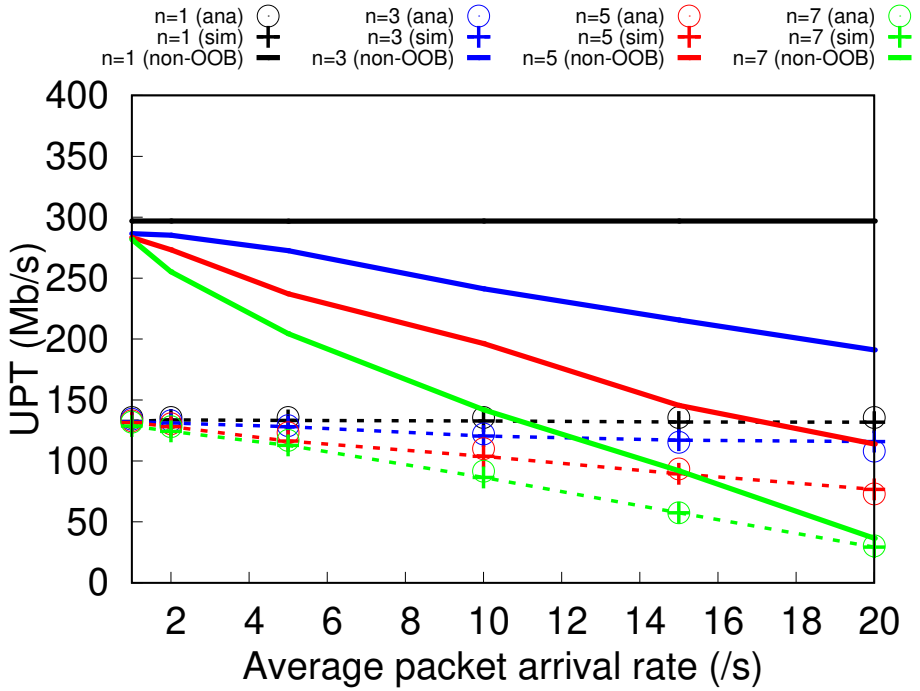
Figure 3.8: UPT performance analysis using the proposed Markov model in an OOBE environment in 4 carriers.

narrows the choice of carriers. We introduce an energy detection algorithm considering OOBE which our scheme uses to access AACs even when they are located near AOCs.

Wi-Fi and LTE-LAA use the energy detection algorithm to sense carriers. The energy of the detected signal can be expressed as

$$E = \frac{1}{N} \sum_{n=0}^{N-1} |y[n]|^2. \tag{3.11}$$

E is the energy of the detected signal, $y[n]$ is the detected signal at time n, and $N = f_s \sigma$, where f_s is the sampling rate and σ is the energy detection time. The device collects time-sampled signals during the energy detection time and averages the energy

of the collected signals. Converting the sampled signal into the frequency, we have

$$Y[k] = \sum_{n=0}^{F_s\sigma-1} y[n]exp(-j2\pi nk/F_s\sigma).$$ (3.12)

Then we can derive the frequency spacing Δf and the sampled signal bandwidth BW_s, respectively, as

$$\Delta f = \frac{2\pi}{N}\frac{f_s}{2\pi} = f_s N$$ (3.13)

and

$$BW_s = f_s.$$ (3.14)

Since the sampled signal has the same bandwidth with F_s, we have[5]

$$E = \frac{1}{(BW_s/\Delta f)} \sum_{k=0}^{BW_s/\Delta f-1} Y[k].$$ (3.15)

Therefore, the energy detection in Wi-Fi can detect only the operating bandwidth, while that in LTE-LAA can detect a larger bandwidth than the operating bandwidth.

3.4.1 Energy Detection Algorithm

We measured signals on AAC while the eNB is transmitting on AOC using NI USRP-2943R that has Xilinx Kintex-7 FPGA, using LabVIEW communication system design suite (CSDS) and LTE-LAA application framework [46]. Fig. **??**(a) shows the measured received power spectrum density on AAC where AOC has 20 MHz higher carrier frequency. The energy of the transmitted signal on AOC is observed over 10 MHz. [6] If the AAC is located near AOC, it suffers interference from not only OOBE but also AOC transmission.

---

[5] F_s is 20 MHz in Wi-Fi that equals the operating bandwidth, but in LTE-LAA it is 30.72 MHz which is larger than the operating bandwidth.

[6] The energy below -10 MHz is the result of aliasing, and the energy on the center carrier frequency comes from local oscillator leakage given by the device specification.
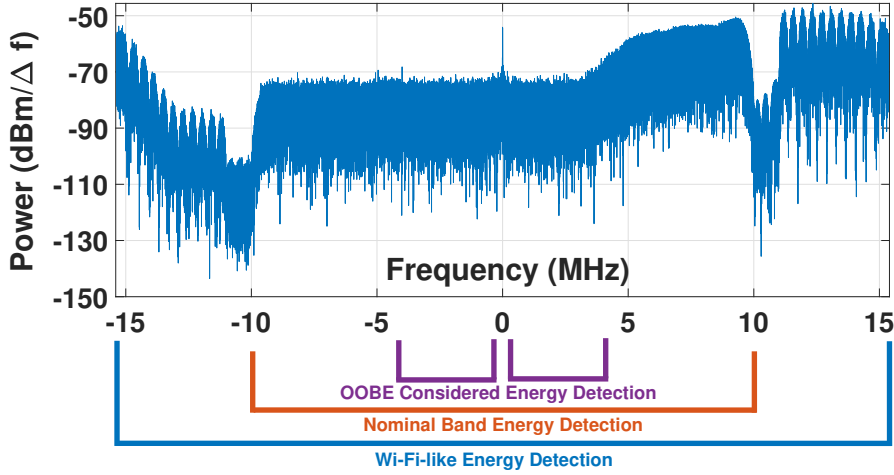
Figure 3.9: OOBE measurements on USRP-2943R in the frequency domain.

3.4.2 Nominal Band Energy Detection

In [19], ETSI regulates the detected energy level as the energy integrated over the nominal channel bandwidth, which is the widest band of frequencies, assigned to a single channel which is 20 MHz in LTE-LAA. To meet the regulation, we cut off the energy in the frequency domain and express the nominal band energy detection as

$$E_N = \frac{1}{(BW_N/\Delta f)} \sum_{k=f_{LN}}^{f_{UN}} Y[k], \qquad (3.16)$$

where BW_N is the nominal channel bandwidth 20 MHz, $f_{LN} = (BW_s - BW_N)\Delta f/2$ where the sample number denotes the lower frequency of the nominal band, and $f_{UN} = (BW_s - BW_N)\Delta f/2 + BW_N - 1$ where the sample number denotes the upper frequency of the nominal band. Differently from the Wi-Fi-like energy detection mechanism, the nominal band energy detection (NBE) should pass signals through fast Fourier transform (FFT).[7] The NBE can weaken the signals transmitted by AOCs, but OOBE still exists in the nominal band. Therefore, the NBE cannot judge correctly

---

[7]According to [47], passing the signal through the FFT is acceptable because the execution time of the FFT is short enough to decide whether carrier is busy or not.
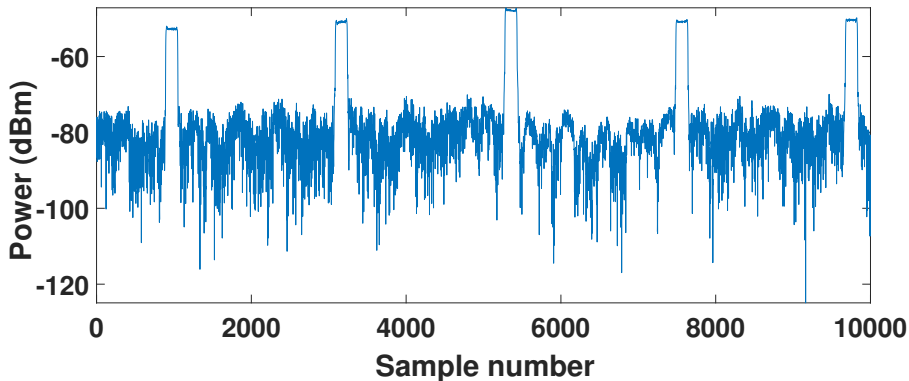
Figure 3.10: OOBE measurements on USRP-2943R in the time domain.

whether the carrier is idle or busy due to OOBE.

3.4.3 OOBE-Free Region Energy Detection

To overcome OOBE leakage from AOC, we propose an OOBE-free region energy detection algorithm. In Fig. **??**(a), there is OOBE from 4 MHz to 10 MHz, while there is no OOBE from -10 MHz to 4 MHz. If the center frequency of AOC is lower than that of AAC, OOBE exists from -10 MHz to -4 MHz. The proposed algorithm operates on the carrier using a frequency band not affected by OOBE and uses the following.

$$E_O = \frac{BW_N}{BW_O} \sum_{k=f_{LO}}^{f_{UO}} Y[k], \tag{3.17}$$

where E_O is the estimated nominal band carrier energy and BW_O is the bandwidth from f_{LO} to f_{UO}. f_{LO} and f_{UO} are the sample numbers at -4 MHz and 4 MHz, respectively.[8] The energy detection above may underestimate signals because no-signal area whose frequency is the center carrier frequency is multiplied. Excluding the center

---

[8]Most off-the-shelf devices using OFDM do not transmit signals at the center carrier frequency due to DC offset, which is caused by the energy leakage in the RF front-end [48].

carrier frequency from OOBE free region, we can rewrite E_O as

$$E_O = \frac{BW_N}{BW_O - 1} \sum_{\substack{k=f_{LO} \\ k \neq f_s/2}}^{f_{UO}} Y[k], \tag{3.18}$$

where the sample number of the center carrier frequency is $f_s/2$. Fig. **??**(b) shows OOBE measurement results on USRP-2943R in the time domain. OOBE is observed only at the boundary of the symbols because OOBE occurs due to the discontinuity between OFDM symbols [42]. Since the RF modules operating on AOC and AAC are installed in the same unit, the eNB can know the boundary of symbols on AOC. The proposed energy detection algorithm senses carriers using NBE and the CCA slot does not cross the boundary of symbols. When the CCA slot crosses the boundary of symbols, the eNB senses carriers using OOBE free region energy detection not to be affected by OOBE.

3.5 Additional Carrier Access Scheme

In this section, we propose a novel carrier access scheme for LTE-LAA to enhance channel efficiency. We consider regulation issues and characteristics of the unlicensed band to make the proposed scheme more practical.

3.5.1 Basic Operation

Our scheme enables the eNB to occupy additional idle carriers that were busy when the eNB starts transmitting. In Fig. 3.11, the eNB starts transmitting on the upper carrier right after LBT operation. However, it cannot start transmitting on the lower carrier because the lower carrier is busy due to Wi-Fi traffic at that time.

The legacy scheme allows transmission only on the AOCs until the transmission burst ends. However, our scheme allows the eNB to keep sensing AACs. When an AAC becomes idle, the eNB starts LBT operation independently to access it. After
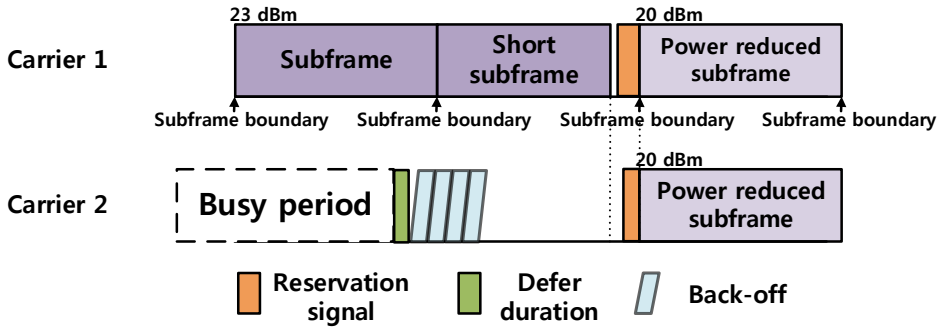
Figure 3.11: Overview of the additional carrier access scheme.

the LBT operation is completed, the eNB waits for the closest subframe boundary to appear. If the AAC is still idle at the subframe boundary, the eNB starts transmitting on it.

3.5.2 Transmission Power Limitation

The ETSI defines the limitation of RF output power for devices operating in the 5 GHz unlicensed band [19]. Due to this rule, the eNB should split its transmission power across multiple carriers to allow additional carrier access. The 3GPP regulates that the signal strength cannot be changed within one transmission burst because the user equipment (UE) estimates the channel by measuring the reference signal. This regulation makes it difficult to set the transmission power to the maximum at the start of transmission because the transmission power should be changed when the eNB accesses an additional carrier. Although we next explain the use of one AAC for simplicity, we can allow up to three AACs in the unlicensed band according to the 3GPP Release 10.

To overcome the transmission power reduction problem[9] to occupy an uncertain number of additional carriers, we propose to divide one transmission burst into multiple ones, which allows the eNB to always transmit the signal with the maximum

---

[9]For example, the eNB should set the per carrier transmission power to 6 dB lower when occupying three additional carriers.

transmission power by changing the per carrier transmission power within one channel occupancy time.

3.5.3 Dividing Transmission Burst

When an additional carrier is sensed as idle, the eNB schedules a short subframe on AOC, which is placed right before the time the eNB wants to access AAC. The length of a short subframe is one symbol shorter than a subframe. Due to the time gap of one symbol between the end of the short subframe and the next subframe boundary, the eNB is allowed to divide one burst into multiple ones and change its transmission power per carrier.

To prevent other devices from occupying this carrier during this time gap, the eNB transmits a reservation signal on the AOC (RS_{AOC}) right before the following subframe. In 5 GHz unlicensed band, other than the Wi-Fi acknowledgement frame can not occupy the channel during the short interframe space (SIFS) period whose length is 16 μs. Since LTE-LAA is LTE based technology and operates in the unlicensed spectrum, multiple eNBs may start transmission at the time of the subframe boundary, resulting in a collision. The eNB to access an AAC transmits a reservation signal RS_{AAC} to avoid collision. The length of RS_{AAC} is set to an arbitrary value between the end of the short subframe and the following subframe boundary.

3.5.4 Short Subframe Decision

In order to transmit a short subframe, the eNB needs to determine the length and transmission time of the short subframe. Short subframe transmission creates a time gap between the end of the short subframe and the start of the next subframe. If the length of the short subframe is too small, the length of the time gap becomes large. The large time gap needs long RS_{AOC} because RS_{AOC} should fill the empty channel to prevent other devices from occupying the AOCs. Since the reservation signal has no data, a longer duration of RS_{AOC} degrades network throughput.
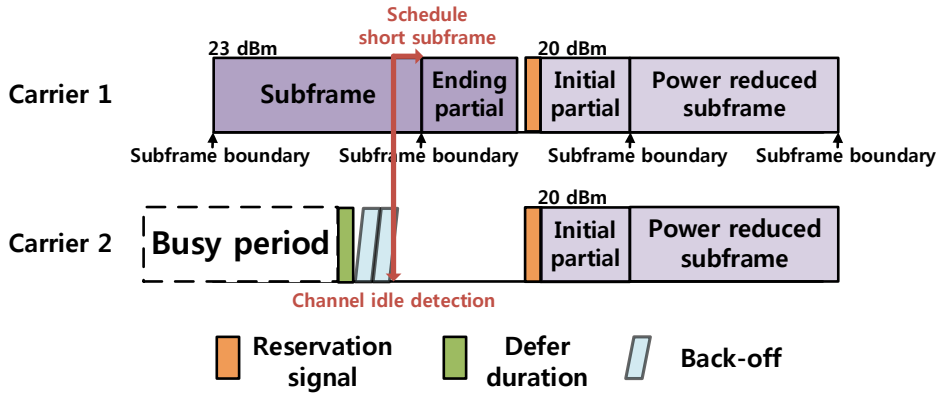
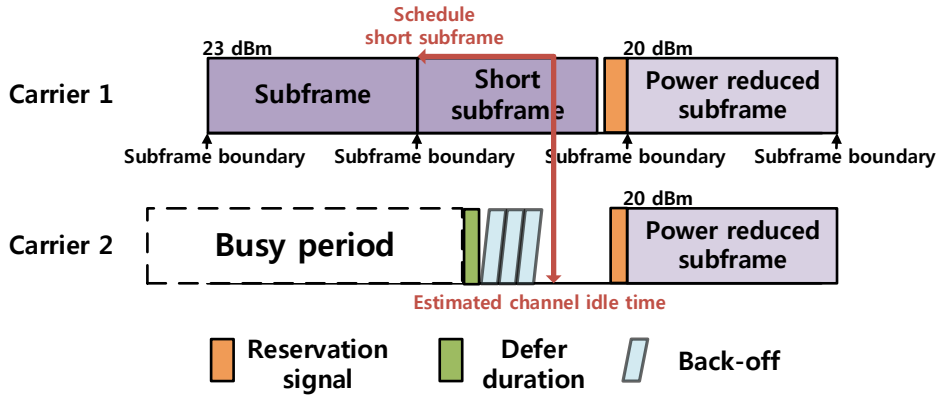Figure 3.12: Scheduling a short subframe right after the AAC becomes idle.

Figure 3.13: Estimating the busy period for scheduling a short subframe.

If the length of the short subframe is too long, the chance of selecting RS_{AAC} is low and the possibility of collision increases. RS_{AAC} is similar to the back-off counter value in CSMA/CA whose contention window size is the time gap. The proposed scheme reduces the short subframe duration by one symbol if a collision occurs on the AAC such as doubling the contention window size.[10]

Since short subframe transmission causes network throughput degradation due to

---

[10]One symbol duration of LTE-LAA is 71.6 μs which is almost 8 clear channel assessment (CCA) slot duration. Therefore, reducing the length of the short subframe by one symbol duration has the same effect as doubling the contention window size for the first time in CSMA/CA.

the time gap, the eNB should schedule short subframes as little as possible. Fig. **??**(a) illustrates the first case that the method schedules a short subframe right after the AAC becomes idle. After the busy period ends in the AAC, the eNB schedules the following subframe as a short subframe if the back-off counter reaches zero before that time. However, in this case, the channel is wasted because the eNB cannot transmit any signal until the ending time of the short subframe.

To avoid channel waste, the eNB schedules the short subframe as an ending partial subframe rather than one symbol reduced subframe.[11] If the eNB schedules a short subframe as an ending partial subframe whose length is less than 500 μs, it can access the AAC (carrier 2) in the middle of subframe transmission using an initial partial subframe whose length is 500 μs. With the partial subframe transmission, the short subframe decision method helps the eNB to reduce channel waste.

Fig. **??**(b) of the second case shows how the short subframe decision method works when the eNB can estimate when the busy period will end. The eNB schedules a short subframe in advance, further reducing in channel waste. The eNB knows the start time of each busy period because it always senses the AAC. Since the eNB can detect Wi-Fi signals using its own radio-frequency module according to [49], it knows that the busy period is due to Wi-Fi signal or LTE-LAA signal. Therefore, the eNB can estimate the end time of the busy period on the AAC.

Fig. 3.14 illustrates the overall procedures for the short subframe decision by which the eNB determines the short subframe transmission time. At first, the eNB uses the second case of short subframe decision that detects whether the busy period is due to the packet transmission of LTE-LAA or Wi-Fi . Then, the eNB senses the AAC until it is idle. If the AAC becomes idle at the time the eNB expects, the eNB starts transmitting the scheduled short subframe. On the other hand, if the AAC becomes idle before the time the eNB expects, the eNB uses the first case and schedules a short subframe as the following subframe.

---

[11]The subframe length is 14 symbols while that of an ending partial subframe can be 3, 6, 9, 10, 11, 12 symbols [36].

3.6 Performance Evaluation

In this section, we evaluate the performance of the proposed carrier access scheme using ns-3 simulator and validate the performance of the energy detection algorithm considering OOBE through USRP-2943R implementation.

3.6.1 Performance of Energy Detection considering OOBE

We evaluate OCE and NBE on USRP-2943R. We use two USRP devices. Device 1 transmits signals at 5.14 MHz and senses the channel at 5.12 MHz, and device 2 transmits signals at 5.12 MHz and causes interference to device 1. We use the correct decision ratio as the performance metric, and vary the received interference signal strength from -77 dBm to -65 dBm. Note that the energy detection threshold of LTE-LAA is -72 dBm. Device 1 senses the channel 10000 times, and makes a decision whether the channel is 'busy' or 'idle'.

Fig. 3.15 shows the correct decision performance of NBE and OCE. For the interference strength of greater than -69 dBm, NBE and OCE detect the channel as busy with the accuracy of greater than 99%. In the case of -71 dBm, NBE and OCE show low correct decision ratios due to channel fluctuation that cross the energy detection threshold. OCE always shows higher accuracy than NBE because it can exclude OOBE for channel sensing.

3.6.2 Simulation Environments

We use an indoor deployment scenario suggested in the 3GPP technical report 36.889 [50] where two operators place four small cells each, as shown in Fig. 3.16

The two operators use LTE-LAA and Wi-Fi, respectively. The bandwidth per carrier is 20 MHz, and we vary the number of carriers from two to four. We use the indoor hotspot channel model justified in the 3GPP technical report [51], and set the maximum transmission power to 23 dBm [19]. Adopting the low bitrate FTP traffic

Table 3.1: Simulation parameters.

Simulation parameters	Value
Simulation time	10 s
Number of iterations	30
λ	$1 - 5$ (/s)
Wi-Fi PHY	802.11ac, 2×2 MIMO
maximum Wi-Fi A-MPDU bound	5.484 ms
LTE-LAA MCOT	8 ms
Wi-Fi rate adaptation	Minstrel VHT
LTE-LAA rate adaptation	AMC
Wi-Fi CS/CCA threshold	-82 dBm
Wi-Fi CCA-ED threshold	-62 dBm
LTE CCA-ED threshold	-72 dBm

model [51], the eNB transmits 500 KBytes files which follow Poisson arrivals with rate λ. The rest simulation settings are shown in Table 3.1.

3.6.3 Performance of Proposed Carrier Access Scheme

We evaluate the proposed carrier access scheme and compare it with the legacy LBT types A and B. Fig. **??**(a) shows that the average UPT of LTE-LAA increases with the number of unlicensed band carriers. LBT type A shows the lowest UPT performance because it cannot use all the carriers efficiently due to OOBE. Furthermore, LBT type A uses low per carrier transmission power due to the uncertainty of the number of accessing carriers.

LBT type B shows better performance than type A because it can access more carriers at first. However, LBT type B also suffers from OOBE. Our proposed scheme always shows the best UPT performance. This is because our scheme can access more additional carriers while the eNB is transmitting. In the case of four carriers, our proposed scheme shows the UPT gains of 59% and 21.5% over LBT types A and B, respectively. Fig. **??**(b) shows the average UPT of Wi-Fi for each LBT. They show almost the same performance. This means that our scheme improves LTE-LAA per-

formance without compromising Wi-Fi performance.

Fig. 3.19 shows the MCS distribution for each LBT type when $\lambda = 3$ for Wi-Fi and LTE-LAA. The MCS distribution of the proposed scheme is higher than that of LBT type A, but lower than LBT type B. The proposed scheme accesses more carriers compared to LBT type B, thereby using lowered average per carrier transmission power.

Fig. 3.20 and Fig. 3.21 show the UPT gain color map. LTE-LAA types A and B show high gain for low λ, and low gain for high λ. High λ makes the channel saturated, resulting in less chance of accessing AACs. In the saturated channel condition, the proposed scheme operates similarly to the legacy LBT type B.

3.7 Summary

We presented a novel multi-carrier access scheme for LTE-LAA that aims to reduce channel waste observed in the conventional multi-carrier operation. We also introduced the energy detection algorithm considering OOBE. The proposed detection algorithm senses the channel with high accuracy even under the existence of OOBE. To this end, our proposed scheme divides a transmission burst into multiple ones and uses short subframe transmission to meet transmission power requirements. Through USRP implementation and ns-3 simulation, we confirm the feasibility of our proposal and its superiority over the legacy schemes. We believe that our work can contribute to overcoming the OOBE problem and improving the channel efficiency of cellular communication in the unlicensed band.
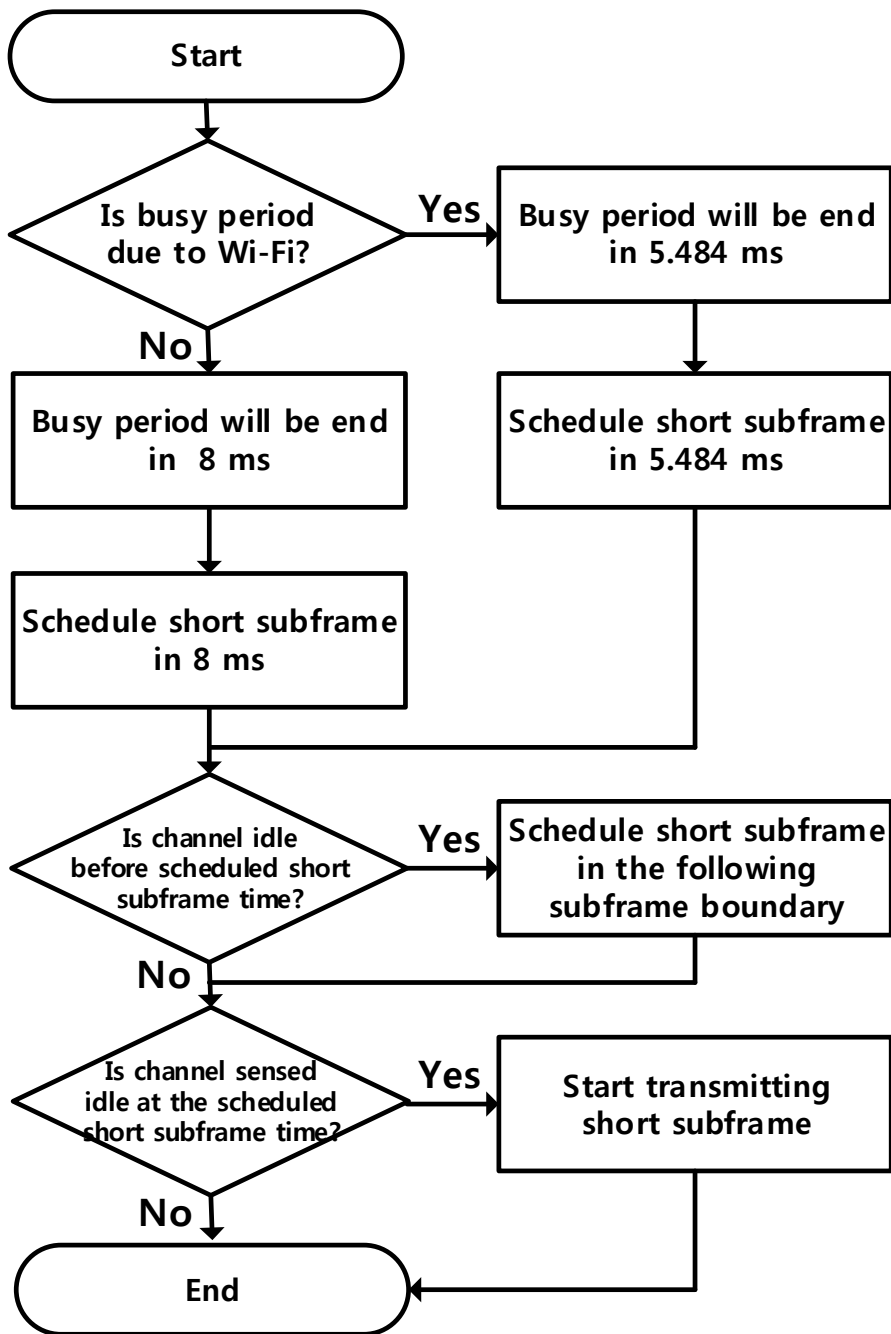
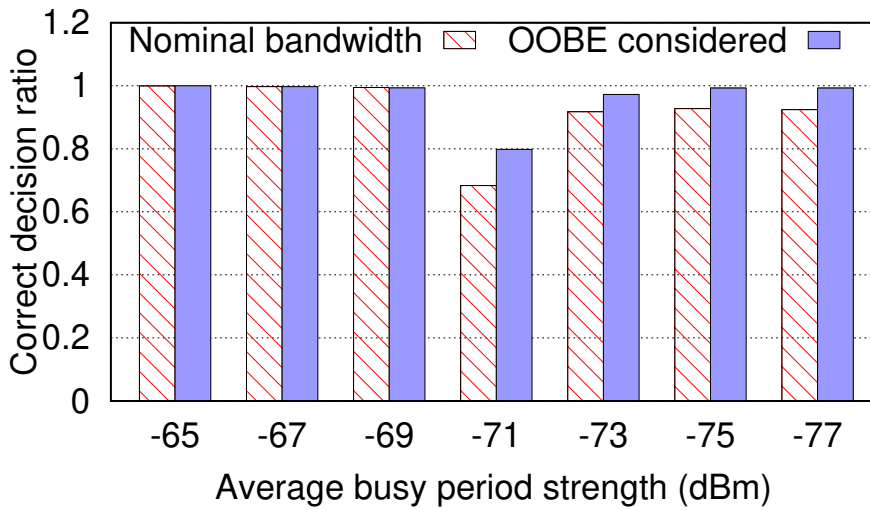Figure 3.14: Short subframe decision block diagram.

Figure 3.15: Correct decision ratio of the energy detection algorithms.
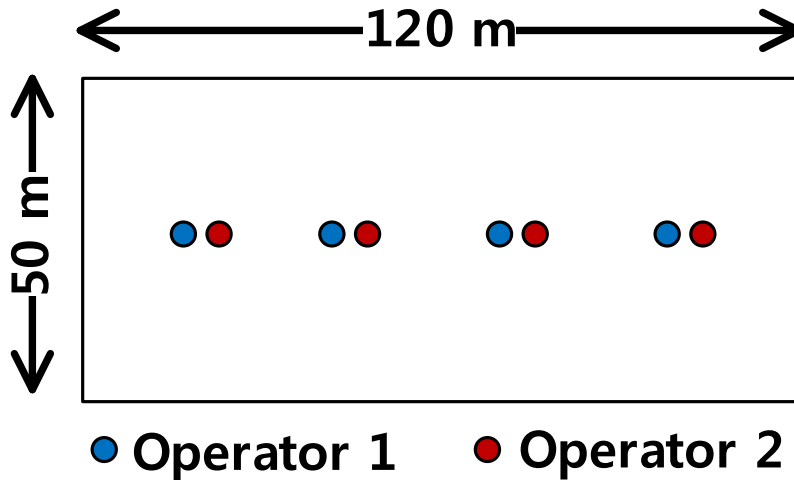

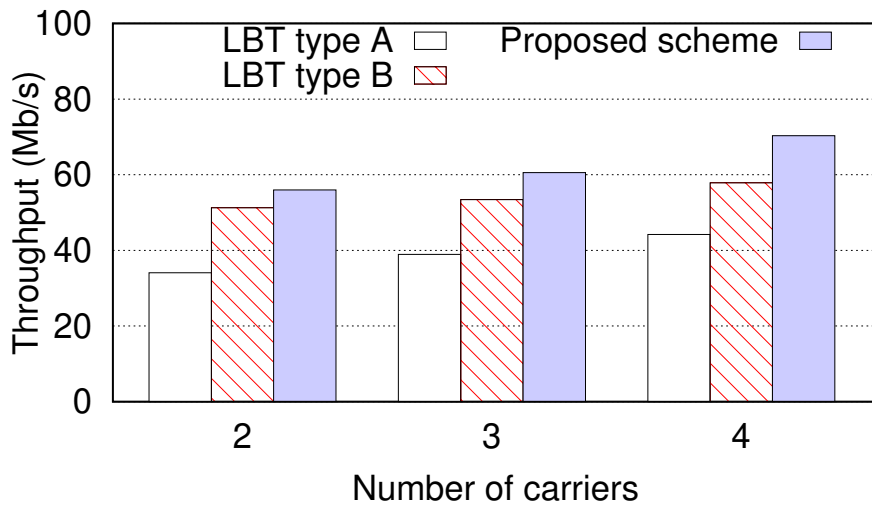Figure 3.16: Indoor deployment scenario.

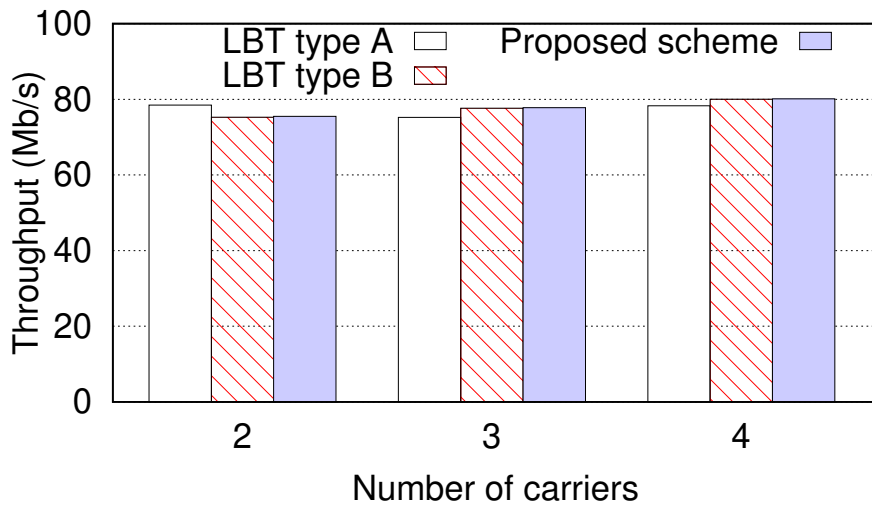Figure 3.17: Average UPT of LTE-LAA for each LBT.

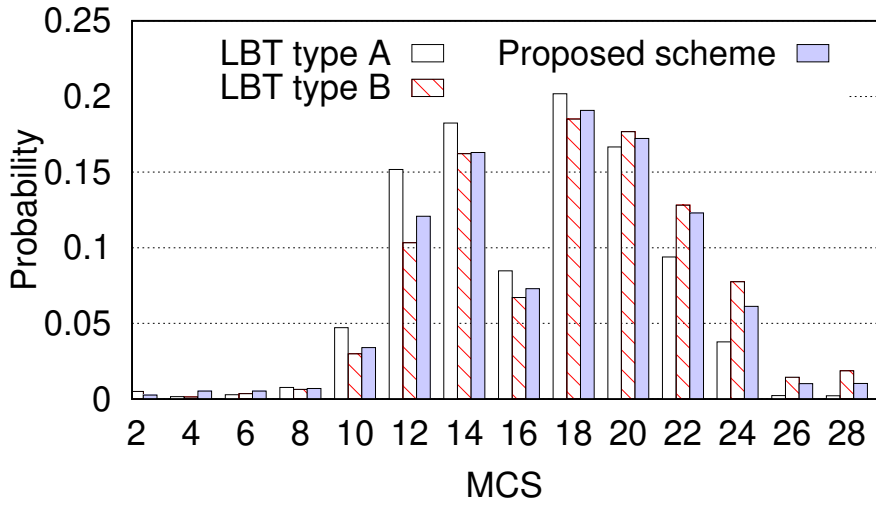Figure 3.18: Average UPT of Wi-Fi for each LBT.
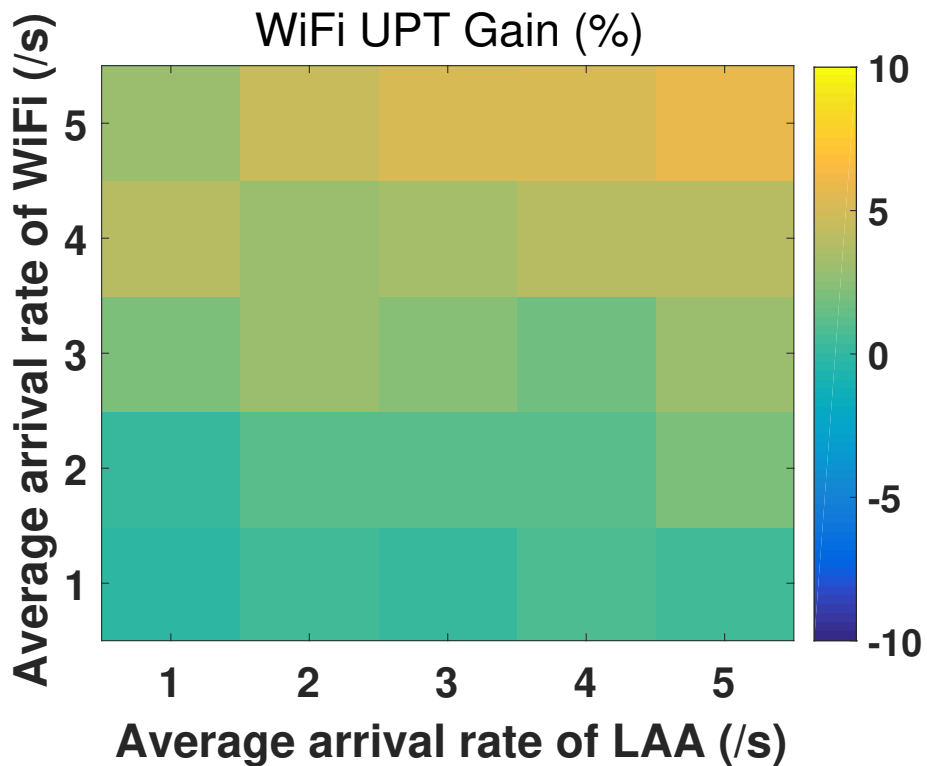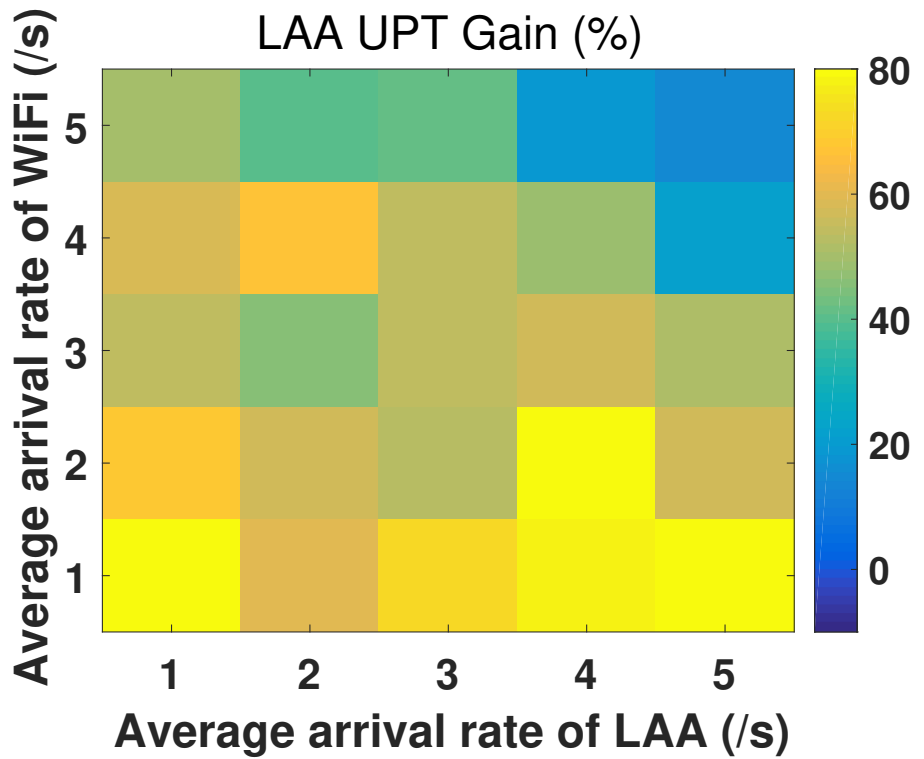
Figure 3.19: MCS distribution for each LBT type.

Figure 3.20: Average UPT gain of LTE-LAA and Wi-fi in LBT type A.
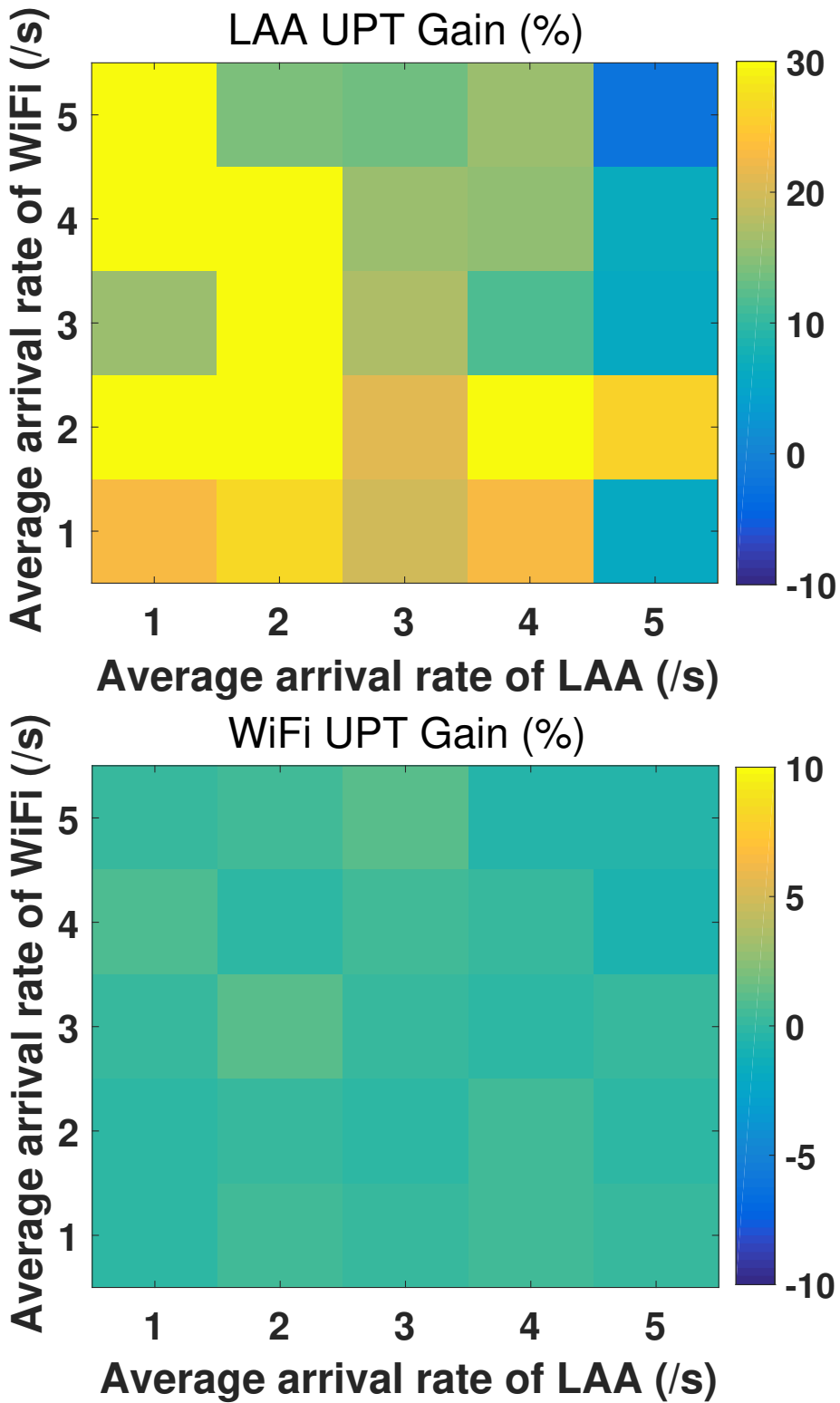
Figure 3.21: Average UPT gain of LTE-LAA and Wi-fi in LBT type B.

Chapter 4

W-ARQ: Wi-Fi Assisted HARQ for Unlicensed Band Stand-Alone Cellular Communication System

4.1 Introduction

As the spread of smart devices becomes active, demand for various applications is increasing as time passes. The most widely used of these applications is video streaming. Video streaming requires a very high data rate, and as video quality increases from the existing 480p to the current 4K, the data rate demand is increasing exponentially. In line with this trend, wireless communication technology has also developed in the direction of using more resources. The unlicensed band is a band that anyone can use at no cost, and many communication technologies use the unlicensed band to use a wider frequency band.

3GPP also proposed a technology called license-assisted access (LAA) to use the unlicensed band in addition to the previously used licensed band. However, LAA is a technology that adds an unlicensed band to the licensed band, and it must be connected to the licensed band eNB through an ideal backhaul. The need for an ideal backhual installation places many limitations on LAA eNB deployment. Therefore, in order to solve this deployment limitation, 3GPP proceeded to move the licensed band technolo-

gies used by LAA to the unlicensed band in sequence. In enhanced LAA (eLAA), the uplink data transmission that was transmitted from the LAA to the licensed band can be transmitted to the unlicensed band.

For this, eLAA proposed an uplink listen-before-talk (LBT) operation. The uplink LBT operation proposed by eLAA includes category 2 and category 4 LBT, and category 2 LBT is used when uplink transmission is performed within a predetermined channel occupancy time (COT). Category 4 LBT is performed when transmitting uplink beyond COT. Also, for uplink transmission, an interlace structure was proposed by modifying single carrier frequency division multiple access (SC-FDMA), an uplink operation of the existing LTE.

Further enhanced LAA (feLAA) proposed a grant free uplink capable of performing uplink transmission without scheduling of an eNB by further supplementing eLAA. In addition, feLAA solved the deployment constraints by replacing the carrier aggregation technology that requires an ideal backhaul with dual connectivity technology, but dual connectivity alone is not completely free of the deployment constraints.

Therefore, MulteFire alliance proposed MulteFire, an unlicensed band stand-alone technology based on LAA, to solve deployment limitations. Unlike eLAA and feLAA, MulteFire operates only in the unlicensed band, so the uplink control message transmitted from eLAA and feLAA to the licensed band can be operated in the unlicensed band.

4.2 Background

MulteFire, proposed by the MulteFire alliance, is a stand-alone communication technology in the unlicensed band, and all signals are transmitted in the unlicensed band. In particular, control messages that were impossible in LAA, eLAA, and feLAA are transmitted to the unlicensed band. For this purpose, MulteFire proposed a new frame. The physical uplink channel (PUCCH), which was used to transmit the control mess-

sage in the existing LTE, was divided into short PUCCH (sPUCCH) and extended PUCCH (ePUCCH) to be used in the unlicensed band. sPUCCH uses the last 4 symbols in the entire subframe, and the 10 symbols located in front are not used for uplink. In general, the sPUCCH exists after the downlink ending partial subframe and is used to switch from downlink to uplink. Since sPUCCH comes after the downlink ending partial subframe, it reduces the LBT gap for uplink transmission. By reducing the LBT gap, more uplink transmission opportunities can be given. In addition, since sPUCCH uses 4 symbols, it is suitable for transmitting small payload size control messages such as ACK/NACK. ePUCCH uses 14 symbols the same as the existing LTE subframe. Compared to sPUCCH, ePUCCH can contain more information because it uses more symbols. Therefore, ePUCCH is used to transmit a large payload size control message. Since the uplink subframe has an interlace structure, resource waste is minimized by allocating ePUCCH and PUSCH to various interlaces in one subframe.

MulteFire basically uses a scheduling scheme similar to LTE for uplink transmission in an unlicensed band. However, due to the nature of the unlicensed band, uplink transmission may not be properly performed due to LBT failure. Therefore, while LTE operating in the licensed band schedules uplink transmission after 4 subframes, MulteFire supports more flexible delay times. In addition, due to the limited channel occupancy time, MulteFire supports one uplink grant to schedule multiple uplink subframes, and schedules the same data in multiple subframes to perform more robust uplink transmission against LBT failure. The DL HARQ operation is also based on the LTE operation similar to uplink scheduling. However, since ACK/NACK may be difficult to properly transmit due to LBT failure, MulteFire pending ACK/NACK so that it can be transmitted to multiple subframes. In addition, ACK/NACK can be transmitted through both sPUCCH and ePUCCH, thereby improving robustness. In order to further improve the ACK/NACK transmission success rate, MulteFire can further increase the transmission opportunity of ACK/NACK by using the flexible frame structure.

4.3 Motivation

We investigated the success rate of MulteFire's uplink control message transmission through simulation. We measured the probability that the sPUCCH can transmit when MulteFire's sPUCCH periodically exists and the length of the ePUCCH that is transmitted on average when the ePUCCH is scheduled for 4 subframe lengths as an uplink grant.

In [52], the authors analyzed the transmission probability of sPUCCH and ePUCCH. Both PUCCH transmission can be disturbed by interference due to the nature of unlicensed band. When the duration of interference is 1 ms, the transmission probability of sPUCCH is up to 6.5% when the contending node is only one. However when the contending nodes increases, the transmission probability is less than 3%. Also when the interference duration becomes longer, the transmission probability of sPUCCH becomes almost zero. When the duration of interference is 1 ms, expected length of ePUCCH is more than 1 ms. However since the scheduled ePUCCH duration is 4 ms, the transmission probability is also low. Moreover when the duration of interference becomes longer and the number of contending nodes increases, expected duration of ePUCCH becomes almost zero. Therefore we can notice that the conventional Multe-Fire has poor uplink control message transmission performance.

4.4 W-ARQ: Wi-Fi assisted HARQ for Unlicensed Band Stand-Alone Cellular Communication System

Due to the poor performance of existing unlicensed band stand-alone cellular communication system, we propose novel uplink control message transmission method which called W-ARQ. W-ARQ is Wi-Fi assisted HARQ for unlicensed band stand-alone cellular communication system. W-ARQ divides the channel occupancy time into two parts. The first part is the transmission of the existing LAA, and the LAA subframe is transmitted. The second part is the part where the LAA has finished transmitting,
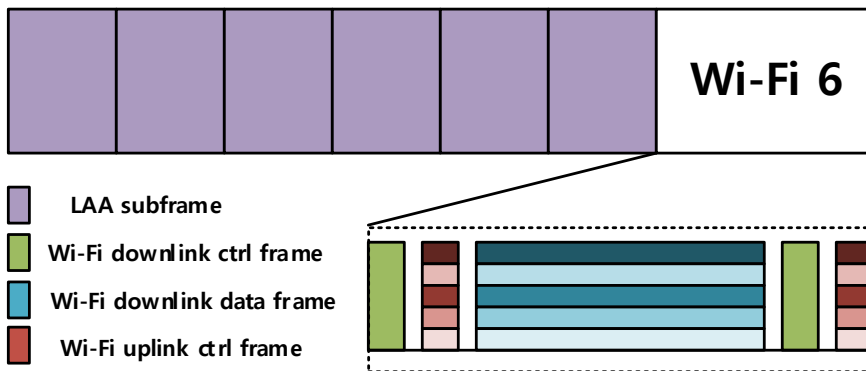
Figure 4.1: Basic operation of W-ARQ.

and performs Wi-Fi transmission. Wi-Fi transmission supports downlink OFDMA by applying the Wi-Fi 6 protocol and allocates resources similar to downlink OFDMA transmitted by the existing LAA to the terminals. The Wi-Fi transmission part includes request to send (RTS) and clear to send (CTS) frame transmission, and includes block ACK request (BAR) and block ACK frame transmission. That is, when LAA transmission is finished, the RTS is transmitted by the base station. Terminals that receive this transmit CTS to inform them that Wi-Fi transmission is ready. Thereafter, the base station transmits a Wi-Fi data packet, and then the base station transmits a BAR. Thereafter, the UE transmits a block ACK to end one DL burst. W-ARQ uses block ACK of Wi-Fi as ACK/NACK of LAA transmission. Accordingly, the LAA base station can determine whether the previous LAA transmission has failed by receiving the block ACK of Wi-Fi. Fig. 4.1 shows the proposed W-ARQ operation. Furthermore, W-ARQ chooses conservative MCS when it uses Wi-Fi. Therefore Wi-Fi transmission in W-ARQ is suitable for reliability sensitive services. In V2X communication, there exist control messages which are important for safety named cooperative awareness message (CAM) and decentralized environmental notification message (DENM). Due to the importance of these messages, both Wi-Fi based V2X communication, dedicated

short range communication (DSRC), and cellular communication based V2X commu-niation, cellular-V2X (C-V2X), transmit these messages. However, DSRC and C-V2X has different frame structure. Therefore, in [53], the authors proposes CAM/DENM relaying algorithm dividing frequency band for each communication technology. By using W-ARQ, this can be achieved without divide frequency band. Another reliability sensitive service is power save mode. LTE support discontinuous reception (DRX) to save battery of UE. However in unlicensed band, it is difficult to notice every DRX on/off duration to UE. Thanks to the power save mode of Wi-Fi, LTE-LAA UE can save the battery using this power save mode transmitting beacon frame in Wi-Fi trans-mission of W-ARQ. Moreover, the beacon frame in Wi-Fi transmission of W-ARQ can make unassociated UE to associate the eNB using Wi-Fi association procedure. Because initial random access of LTE-LAA is almost impossible in unlicensed band stand-alone system, this can help the UEs to initially access the eNB.

4.4.1 Parallel HARQ

LAA's ACK/NACK determines whether subframe transmission fails. If transmission is successful, the next data packet is transmitted, and if transmission is unsuccessful, the failed subframe is transmitted again. Therefore, in W-ARQ, the Wi-Fi block ACK must inform the base station of the success or failure of each subframe of LAA. Wi-Fi block ACK has 7 bits that are allocated in the standard but are not used. In addition, the maximum channel occupancy time of LAA is 8 ms, and if the Wi-Fi operation is performed for 2 ms, a total of 6 LAA subframes can be transmitted. Therefore, these 7 bits can contain whether the transmission of 6 subframes has failed.

However, unlike Wi-Fi, which uses convolutional codes, LAA uses turbo codes with high complexity. Turbo code takes longer to decode than convolutional code be-cause of its high complexity. The Wi-Fi block ACK existing in the same DL burst is transmitted at a time too early to include whether the decoding of the LAA subframe has failed. Therefore, the ACK/NACK of the LAA subframe cannot be included in
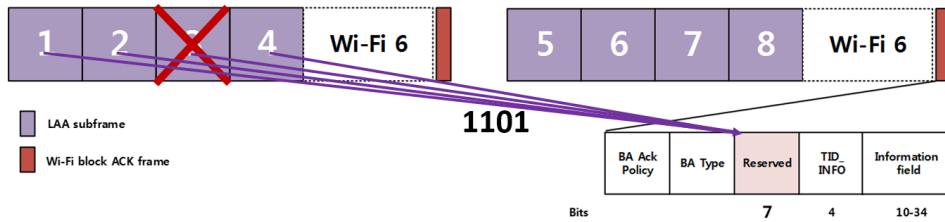
Figure 4.2: Basic operation of parallel HARQ.

the Wi-Fi block ACK existing in the same DL burst. Therefore, we propose parallel HARQ. Paralle HARQ stores whether the transmission of LAA subframes has failed or not in the Wi-Fi block ACK existing in the next DL burst, not the Wi-Fi block ACK existing in the same DL burst. Therefore, since the success or failure of the previous DL burst is not known, the next DL burst continues to transmit without retransmission, and retransmits the subframe that failed in the second previous transmission in the next DL burst. Fig. 4.1 shows the proposed paralle HARQ operation.

4.4.2 Clustered Minstrel

Existing cellular communication uses an adaptive coding and modulation (AMC) operation to determine a transmission rate. The AMC operation measures the SINR of a reference signal present in a downlink subframe when the terminal receives downlink transmission. Channel quality information (CQI) is calculated based on this SINR value. The UE informs the BS of the current channel state by transmitting the calculated CQI at the next ACK/NACK transmission. Based on the received CQI, the base station may select the next transmission MCS.

However, in the W-ARQ operation, only whether the transmission of each subframe has failed successfully can be included in the Wi-Fi block ACK, and there is no free space to contain channel state information. Therefore, the W-ARQ operation cannot use the AMC used by the existing LAA, and instead must perform a rate adaptation operation similar to the method used by the Wi-Fi. Typical rate adaptations of

Wi-Fi are adaptive rate fallback (ARF) and minstrel.

ARF is a simple operation that increases the data rate when transmission is successful and lowers the data rate when transmission fails. ARF determines that if the previous transmission fails twice in succession, it is not an error due to collision, but an error due to channel state change and lowers the data rate. When increasing the transmission data rate, if 10 consecutive data packets succeed, it is judged that the channel status has improved and the data rate is increased. . This is the simplest method, but due to the nature of wireless communication, the channel changes rapidly and the user moves frequently, so it cannot keep up with the rapid channel change well.

Minstrel is a rate adaptation method that operates based on statistics. Statistics are collected every 100 ms, and based on the statistics, the MCS to be transmitted during the next 100 ms is selected. For each 100 ms, a total of four MCSs are selected, and each MCS has characteristics of maximum throughput, second maximum throughput, best probability, and basic rate, respectively. And whenever transmission fails, the data rate is lowered in order to transmit. Minstrel goes through a sampling process to select a transmission MCS for the next 100 ms. Every 10th packet is randomly selected from among MCSs other than the currently transmitted MCS and transmitted, and the success or failure at this time is reflected in statistics. Based on the statistics of the sampled MCSs, four MCSs to be transmitted during the next 100 ms are selected. In the case of Wi-Fi, the number of MCSs used is 10, but in the case of LAA, the number of MCSs is 29. Therefore, the number of MCSs to be sampled is very large. If all these MCSs are sampled for 100 ms, the number of samples for each MCS is unreliably small. Increasing the statistic time to more than 100 ms makes it more susceptible to channel changes. Therefore, the existing Minstrel is not suitable for unlicensed band cellular communication.

We propose a clustered mind to overcome the limitations of the existing rate adaptation of Wi-Fi. Since the existing Minstrel is not suitable for unlicensed band cellular communication with many MCSs, we have reduced the number of MCSs we want to

collect statistics for. Create a cluster by reducing the MCS that collects statistics for 100 ms, and execute the Minstrel operation in this cluster. Due to this operation, the number of MCSs to be sampled is reduced, which achieves an improvement in the reliability of samples. After collecting statistics for 100 ms, based on these statistics, select the cluster to be used for the next transmission. Because clustered Minstrel cannot sample all MCSs, it does not know the performance of MCSs that do not exist in the cluster. Therefore, clustered Minstrel estimates the average SINR value over 100 ms based on statistics as,

$$E[SINR] = mapping(MCS, p), \tag{4.1}$$

where $E[SINR]$ is expected SINR, MCS is used MCS over 100 ms, p is the transmission success probability of used MCS and $mapping$ is a function that maps SINR through BLER curves using MCS and success probability. BLER curves are determined by the hardware specification. Based on the estimated SINR value, the expected throughput that possible clusters can have is calculated by

$$E[T_i] = \sum_{j=i-k/2} i + k/2(MCS_j, p_j), \tag{4.2}$$

where $E[T_i]$ is expected throughput of cluster i, k is a size of cluster, and p_j is a transmission success probability of MCS_j which can be obatained from BLER curves. Channel changes are followed by using the cluster with the highest value among the calculated expected throughput for the next 100 ms such that
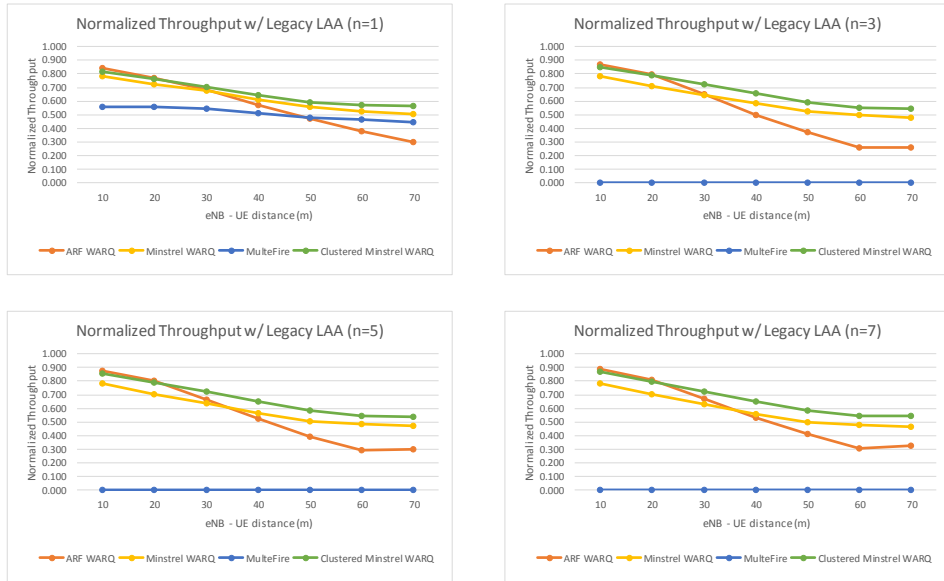
$$C = argmax_i(E[T_i]). \tag{4.3}$$

Figure 4.3: Normalized throughput result of W-ARQ.

4.5 Performance Evaluation

We evaluate proposed W-ARQ using MATLAB simulator. We simulate with 100 seconds and increasing the distance between eNB and UE form 10 m to 70 m. We increase the number of eNBs from 1 to 7, and we compare our proposed scheme with MulteFire, ARF based W-ARQ, and Minstrel based W-ARQ. We used the normalized throughput obtained by dividing the throughput of each technology by the throughput of the LAA transmitting ACK/NACK in the licensed band as a performance verification index. Fig. 4.3 shows the performance of proposed scheme. When there is 1 contending eNB, the proposed scheme has 30%, 7%, 24% higher normalization throughput compared to MulteFire, Minstrel-based W-ARQ, and ARF-based W-ARQ. When there are multiple contending eNBs, MulteFire shows 0 Mbps due to the low probability of PUCCH transmission. In multiple eNB environment proposed scheme shows 14% and 35% higher normalized throughput compared with Minstrel-based W-ARQ and ARF-based W-ARQ.
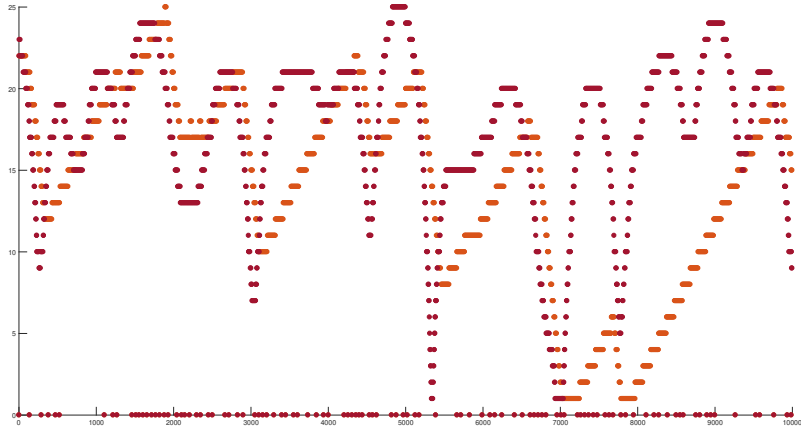
Figure 4.4: MCS selection of ARF.

Fig. 4.4, 4.5, and 4.6 show the MCS selection over time of ARF, Minstrel, and clustered Minstrel rate adaptation algorithm. ARF follows channel slowly. Minstrel has a lot of meaningless samples. However, clustered Minstrel follows channel very well. To verify the performance in various channel environments, we analyzed the performance by varying the Doppler velocity from 5 Hz to 100 Hz.

Fig. 4.7, 4.8, 4.9 show the average normalized throughput, throughput gain compared with ARF and Minstrel under variable Doppler frequencies. Under relatively stable channel condition, ARF shows better performance compared with Minstrel. Minstrel has a lot of meaningless samples, so there is a high probability of choosing the wrong MCS. In a stable channel environment, incorrect MCS selection is fatal to performance degradation. On the contrary, under unstable channel condition, Minstrel shows better performance compared with ARF because ARF cannot follow the channel rapidly. In both stable and unstable channel condition, clustered-Minstrel shows the best performance.
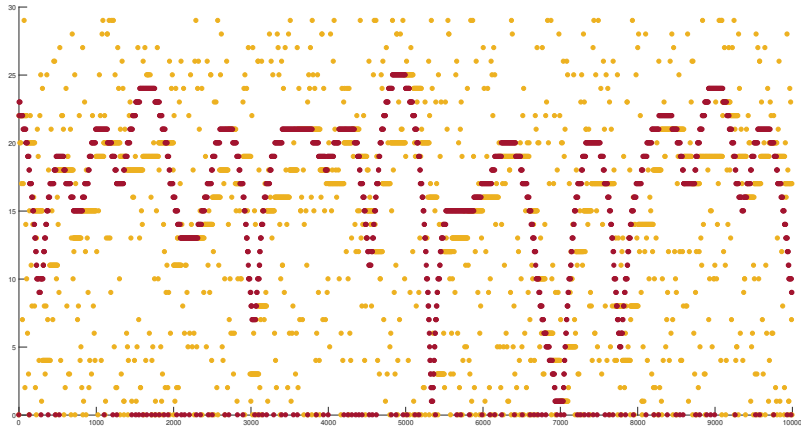
Figure 4.5: MCS selection of Minstrel.

4.6 Summary

We propose W-ARQ, which is Wi-Fi assisted HARQ for unlicensed band stand-alone
cellular communication system. We observed that the conventional MulteFire shows
poor uplink transmsision probability. To overcome the low probability of uplink con-
trol message, we put the uplink control message into Wi-Fi block ACK. To enhance
throughput performance we proposed paralle HARQ, and clustered Minstrel. Our pro-
posed scheme shows higher throughput performance comapred with other shceme.
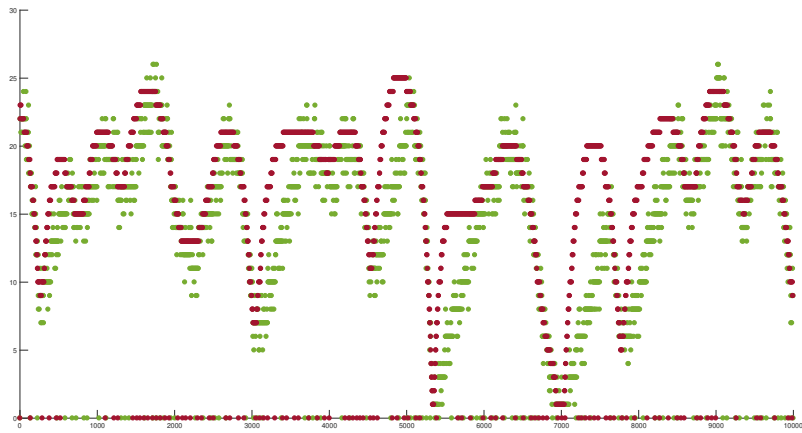
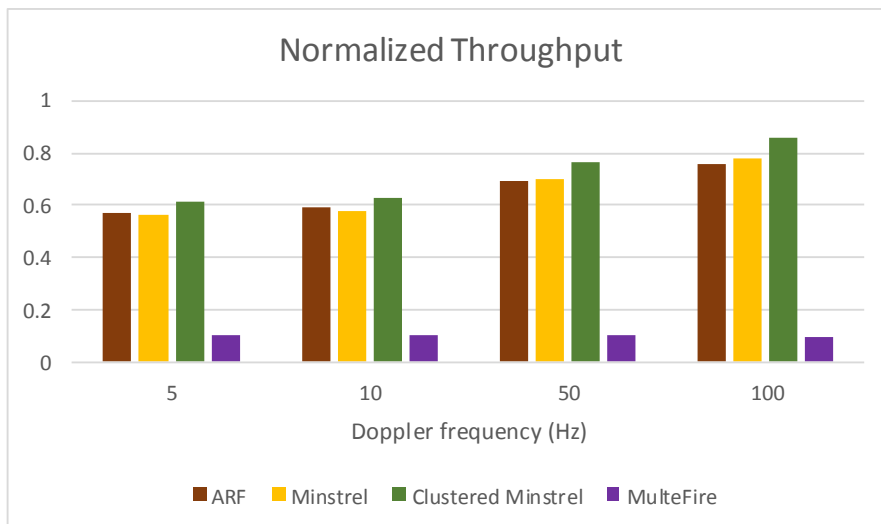Figure 4.6: MCS selection of clustered Minstrel.

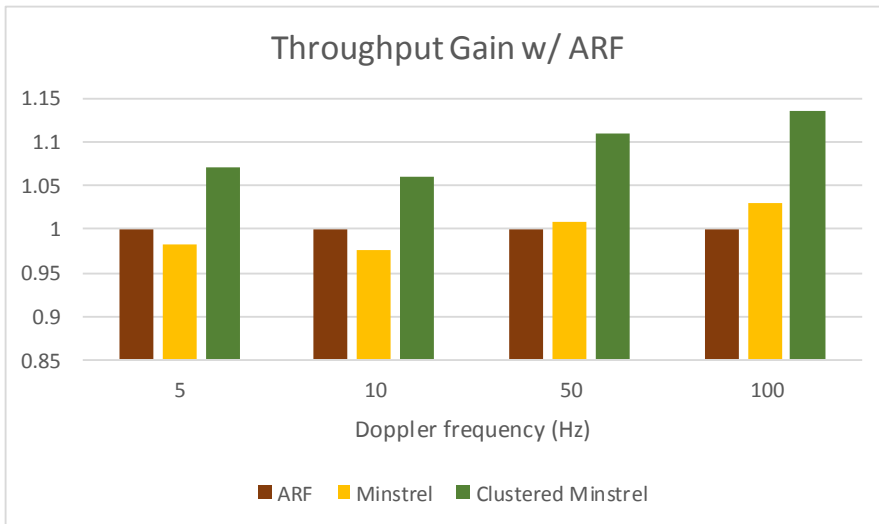Figure 4.7: Average normalized throughput under variable Doppler frequencies.

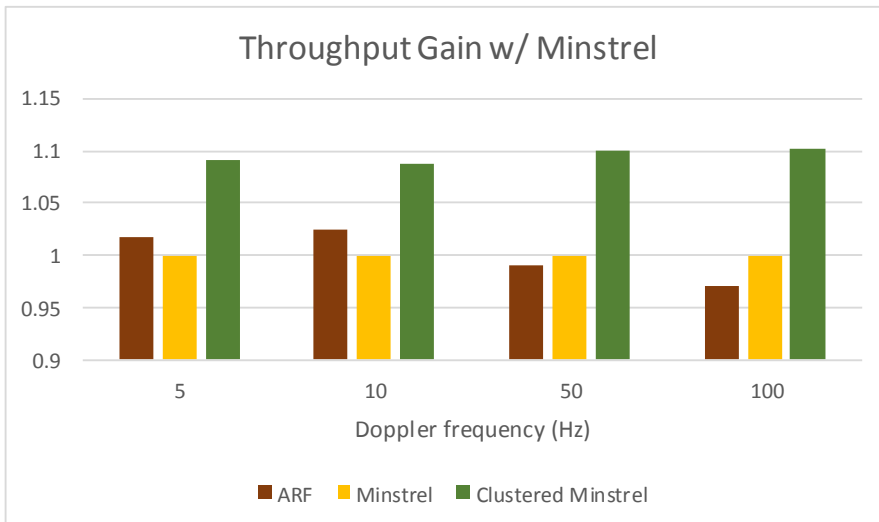Figure 4.8: Average throughput gain compared with ARF.

Figure 4.9: Average throughput gain compared with Minstrel.

Chapter 5

Concluding Remarks

5.1 Research Contributions

In this dissertation, we have addressed

In Chapter 2, we have proposed novel Markov model to analyze LTE-LAA performance under realistic channel model. We found that the LAA transmission has Markov property due to the nature of LBT and newly defined frame structure for LAA. We analyzed AMC under Rayleigh fading model including HARQ operation. The proposed model shows more than 99% accuracy.

In Chapter 3, we have proposed OOBE aware additional channel access for LTE-LAA. We analyzed the impact of OOBE in multi-carrier LAA using Markov model. Then we proposed OOBE considered energy detection method to overcome the impact of OOBE. Lastly we proposed additional carrier access scheme which is fully standard/regulation compliant. Our proposed scheme increases user perceive throughput compared with legacy LAA multi-carrier operation type A and B with average 59% and 22%.

In Chatper 4, we have proposed W-ARQ, which is Wi-Fi assisted HARQ for unlicensed band stand-alone cellular communication system. We observed that the conventional unlicensed band stand-alone cellular communication system has poor uplink

control message transmission probability. Therefore we propose W-ARQ which put uplink control message into Wi-Fi block ACK. We proposed parallel HARQ and clustered Minstrel which enhance W-ARQ acheiving high throughput performance.

5.2 Future Work

As further improvement on the results of this dissertation, there are several research items as follows.

First, additional carrier access algorithm is not suitable for saturated traffic environment. Therefore we are planning to research on-off algorithm of additional carrier access algorithm considering channel busy ratio.

Second, our clustered Minstrel algorithm has fixed cluster size and statistics time. In real, as the channel changes, the optimal cluster size and statistics time will change. We are planning to research cluster size adaptation and statistics time adaptation algorithm for clustered Minstrel rate adaptation.

Lastly, our research is based on LTE-LAA and MulteFire which are from LTE. With the advent of the 5G era, the unlicensed band cellular communication technology is also moving to NR-U. Therefore, our research should also be extended to NR-U.

Bibliography

[1] H.-J. Kwon *et al.*, "Licensed-assisted access to unlicensed spectrum in LTE Release 13," *IEEE Communications Magazine*, vol. 55, no. 2, pp. 201–207, 2017.

[2] G. Bianchi, "Performance analysis of the IEEE 802.11 distributed coordination function," *IEEE J. Sel. Areas Commun.*, vol. 18, no. 3, pp. 535–547, 2000.

[3] Q. Cui, Y. Gu, W. Ni, and R. P. Liu, "Effective capacity of licensed-assisted access in unlicensed spectrum: From theory to applications," *IEEE J. Sel. Areas Commun.*, vol. 35, no. 8, pp. 1754–1767, 2017.

[4] Y. Li, F. Baccelli, J. G. Andrews, T. D. Novlan, and J. Zhang, "Modeling and analyzing the coexistence of licensed-assisted access LTE and Wi-Fi," in *Proc. IEEE Globecom Workshops*, 2015.

[5] Y. Gao, X. Chu, and J. Zhang, "Performance analysis of LAA and WiFi coexistence in unlicensed spectrum based on Markov chain," in *Proc. IEEE Globecom*, 2016, pp. 1–6.

[6] C. Chen, R. Ratasuk, and A. Ghosh, "Downlink performance analysis of LTE and WiFi coexistence in unlicensed bands with a simple listen-before-talk scheme," in *Proc. IEEE VTC*, 2015, pp. 1–5.

[7] C. C. Tan and N. C. Beaulieu, "On first-order Markov modeling for the Rayleigh fading channel," *IEEE Trans. Commun.*, vol. 48, no. 12, pp. 2032–2040, 2000.

[8] Q. Zhang and S. A. Kassam, "Finite-state Markov model for Rayleigh fading channels," *IEEE Trans. Commun.*, vol. 47, no. 11, pp. 1688–1692, 1999.

[9] IEEE 802.11-2012, *Part 11: Wireless LAN medium access control (MAC) and physical layer (PHY) specifications*, IEEE Std., Mar. 2012.

[10] 3GPP, *TS 36.213 v13.5.0 Physical layer procedures release 13*, March 2017.

[11] A. Ghosh and R. Ratasuk, *Essentials of LTE and LTE-A*. Cambridge University Press, 2011.

[12] Y. S. Liaw, A. Dadej, and A. Jayasuriya, "Performance analysis of IEEE 802.11 DCF under limited load," in *Proc. IEEE APCC*, 2005, pp. 759–763.

[13] M. Ergen and P. Varaiya, "Throughput analysis and admission control for IEEE 802.11 a," *Springer Mobile Netw. Appl.*, vol. 10, no. 5, pp. 705–716, 2005.

[14] J. Yi, W. Sun, S. Park, and S. Choi, "Performance analysis of LTE-LAA network," *IEEE Commun. Lett.*, vol. 22, no. 6, pp. 1236–1239, 2017.

[15] M. F. Khan, F. Bhatti, A. Habib, S. Jangsher, I. Zafar, S. Shah, M. Jamshed, and J. Iqbal, "Analysis of macro user offloading to femto cells for 5G cellular networks," 11 2017, pp. 1–6.

[16] M. Salman, M. Abdulhasan, C. Ng, N. Noordin, A. Sali, and B. Ali, "Radio Resource Management for Green 3GPP Long Term Evolution Cellular Networks: Review and Trade-offs," *IETE Technical Review*, vol. 30, p. 257, 05 2013.

[17] J. C. Ikuno, M. Wrulich, and M. Rupp, "Performance and modeling of LTE H-ARQ," in *Proc. International ITG Workshop on Smart Antennas (WSA 2009), Berlin, Germany*, 2009.

[18] ETSI, *EN 301 893 V2.1.0 5GHz RLAN; Harmonized Standard covering the essential requirements of article 3.2 of Directive 2014/53/EU*, March 2017.

[19] E. ETSI, "301 893 V2. 1.1,"5 GHz RLAN; harmonised standard covering the essential requirements of article 3.2 of directive 2014/53/eu,"," *EU," May*, 2017.

[20] A. Anand, G. De Veciana, and S. Shakkottai, "Joint scheduling of urllc and embb traffic in 5g wireless networks," *IEEE/ACM Transactions on Networking*, vol. 28, no. 2, pp. 477–490, 2020.

[21] J. Liu and G. Shen, "Performance of multi-carrier lbt mechanism for lte-laa," in *2016 IEEE 83rd Vehicular Technology Conference (VTC Spring)*. IEEE, 2016, pp. 1–5.

[22] J. Xiao, J. Zheng, L. Chu, and Q. Ren, "Performance modeling of laa lbt with random backoff and a variable contention window," in *2018 10th International Conference on Wireless Communications and Signal Processing (WCSP)*. IEEE, 2018, pp. 1–7.

[23] M. Mehrnoush, S. Roy, V. Sathya, and M. Ghosh, "On the fairness of Wi-Fi and LTE-LAA coexistence," *IEEE Transactions on Cognitive Communications and Networking*, vol. 4, no. 4, pp. 735–748, 2018.

[24] B. Kang, S. Choi, S. Jung, and S. Bahk, "D2D communications underlaying cellular networks on licensed and unlicensed bands with QoS constraints," *Journal of Communications and Networks*, no. 99, pp. 1–13, 2019.

[25] T. Tao, F. Han, and Y. Liu, "Enhanced lbt algorithm for lte-laa in unlicensed band," in *2015 IEEE 26th annual international symposium on personal, indoor, and mobile radio communications (PIMRC)*. IEEE, 2015, pp. 1907–1911.

[26] A. V. Kini, L. Canonne-Velasquez, M. Hosseinian, M. Rudolf, and J. Stern-Berkowitz, "Wi-fi-laa coexistence: Design and evaluation of listen before talk for laa," in *2016 Annual Conference on Information Science and Systems (CISS)*. IEEE, 2016, pp. 157–162.

[27] Z. Ali, L. Giupponi, J. Mangues-Bafalluy, and B. Bojovic, "Machine learning based scheme for contention window size adaptation in lte-laa," in *2017 IEEE 28th Annual International Symposium on Personal, Indoor, and Mobile Radio Communications (PIMRC)*. IEEE, 2017, pp. 1–7.

[28] Y. Son, K. Lee, S. Kim, J. Lee, S. Choi, and S. Bahk, "REFRAIN: promoting valid transmission in high-density modern wi-fi networks," in *Proceedings of the Twenty-First International Symposium on Theory, Algorithmic Foundations, and Protocol Design for Mobile Networks and Mobile Computing*, 2020, pp. 221–230.

[29] X. Gao, H. Qi, X. Wen, W. Zheng, Z. Lu, and Z. Hu, "Energy Detection Adjustment for Fair Coexistence of Wi-Fi and LAA: A Unimodal Bandit Approach," in *2019 IEEE 5th International Conference on Computer and Communications (ICCC)*. IEEE, 2019, pp. 1086–1091.

[30] V. Mushunuri, B. Panigrahi, H. K. Rath, and A. Simha, "Fair and efficient listen before talk (lbt) technique for lte licensed assisted access (laa) networks," in *2017 IEEE 31st International Conference on Advanced Information Networking and Applications (AINA)*. IEEE, 2017, pp. 39–45.

[31] L. Li, J. P. Seymour, L. J. Cimini, and C.-C. Shen, "Coexistence of wi-fi and laa networks with adaptive energy detection," *IEEE Transactions on Vehicular Technology*, vol. 66, no. 11, pp. 10 384–10 393, 2017.

[32] Y. Li, J. Zheng, and Q. Li, "Enhanced listen-before-talk scheme for frequency reuse of licensed-assisted access using lte," in *2015 IEEE 26th Annual International Symposium on Personal, Indoor, and Mobile Radio Communications (PIMRC)*. IEEE, 2015, pp. 1918–1923.

[33] M. Iqbal, C. Rochman, V. Sathya, and M. Ghosh, "Impact of changing energy detection thresholds on fair coexistence of Wi-Fi and LTE in the unlicensed spec-

trum," in *2017 Wireless Telecommunications Symposium (WTS)*.   IEEE, 2017, pp. 1–9.

[34] S. Wang, Q. Cui, and Y. Gu, "Performance analysis of multi-carrier laa and wi-fi coexistence in unlicensed spectrum," in *2017 IEEE/CIC International Conference on Communications in China (ICCC)*.   IEEE, 2017, pp. 1–5.

[35] L. H. Vu and J.-H. Yun, "Power leakage-aware multi-carrier lbt for lte-laa in unlicensed spectrum," in *2018 IEEE International Symposium on Dynamic Spectrum Access Networks (DySPAN)*.   IEEE, 2018, pp. 1–10.

[36] 3GPP, *TS 36.211 v14.4.0 Physical channels and modulation release 14*, September 2017.

[37] X. Huang, J. A. Zhang, and Y. J. Guo, "Out-of-band emission reduction and a unified framework for precoded ofdm," *IEEE Communications Magazine*, vol. 53, no. 6, pp. 151–159, 2015.

[38] E. Güvenkaya, A. Şahin, E. Bala, R. Yang, and H. Arslan, "A windowing technique for optimal time-frequency concentration and aci rejection in ofdm-based systems," *IEEE Transactions on Communications*, vol. 63, no. 12, pp. 4977–4989, 2015.

[39] Y. Zhao and S.-G. Haggman, "Intercarrier interference self-cancellation scheme for ofdm mobile communication systems," *IEEE Transactions on Communications*, vol. 49, no. 7, pp. 1185–1191, 2001.

[40] K. Sathananthan, R. Rajatheva, and S. B. Slimane, "Cancellation technique to reduce intercarrier interference in ofdm," *Electronics Letters*, vol. 36, no. 25, pp. 2078–2079, 2000.

[41] S. Brandes, I. Cosovic, and M. Schnell, "Reduction of out-of-band radiation in ofdm systems by insertion of cancellation carriers," *IEEE communications letters*, vol. 10, no. 6, pp. 420–422, 2006.

[42] R. v. Nee and R. Prasad, *OFDM for wireless multimedia communications*. Artech House, Inc., 2000.

[43] V. Sathya, S. M. Kala, M. I. Rochman, M. Ghosh, and S. Roy, "Standardization advances for cellular and WI-FI coexistence in the unlicensed 5 and 6 ghz bands," *GetMobile: Mobile Computing and Communications*, vol. 24, no. 1, pp. 5–15, 2020.

[44] E. Felemban and E. Ekici, "Single hop ieee 802.11 dcf analysis revisited: Accurate modeling of channel access delay and throughput for saturated and unsaturated traffic cases," *IEEE Transactions on Wireless Communications*, vol. 10, no. 10, pp. 3256–3266, 2011.

[45] 3GPP, *TS 36.104 v14.9.0 Base Station (BS) radio transmission and reception release 14*, March 2019.

[46] "Real-time lte/wi-fi coexistence testbed - national instruments," Mar. 5 2019. [Online]. Available: https://www.ni.com/da-dk/innovations/white-papers/16/real-time-lte-wi-fi-coexistence-testbed.html

[47] M. A. Jaber, D. Massicotte, and Y. Achouri, "A higher radix fft fpga implementation suitable for ofdm systems," in *2011 18th IEEE International Conference on Electronics, Circuits, and Systems*. IEEE, 2011, pp. 744–747.

[48] S. Marsili, "Dc offset estimation in ofdm based wlan application," in *IEEE Global Telecommunications Conference, 2004. GLOBECOM'04.*, vol. 6. IEEE, 2004, pp. 3531–3535.

[49] S.-T. Hong, H. Lee, H. Kim, and H. J. Yang, "Lightweight wi-fi frame detection for licensed assisted access lte," *IEEE Access*, vol. 7, pp. 77 618–77 628, 2019.

[50] 3GPP, *TR 36.889 v13.0.0 Study on licensed-assisted access to unlicensed spectrum release 13*, June 2015.

[51] 3GPP, *TR 36.814 v9.0.0 Further advancements for E-UTRA physical layer aspects release 9*, March 2010.

[52] J. Kim, J. Yi, and S. Bahk, "Uplink Channel Access Enhancement for Cellular Communication in Unlicensed Spectrum," *IEEE Access*, 2020.

[53] B. Kim, S. Kim, H. Yoon, S. Hwang, M. X. Punithan, B. R. Jo, and S. Choi, "Nearest-first: Efficient relaying scheme in heterogeneous V2V communication environments," *IEEE Access*, vol. 7, pp. 23 615–23 627, 2019.

초 록

국문초록 3GPP는 LAA (licensed-assisted access)라고하는 5GHz 비면허 대역 LTE를 개발했습니다. LAA는 충돌 방지 기능을 사용하기 위해 Wi-Fi의 CSMA / CA (Carrier Sense Multiple Access with Collision avoidance)와 유사한 LBT (Listen Before Talk) 작업을 채택하여 각 LAA 다운 링크 버스트의 프레임 구조 오버 헤드는 각각의 종료 시간에 따라 달라집니다. 이전 LBT 작업. 이 논문에서는 비면허 대역 셀룰러 통신을 분석하기위한 수치 모델을 제안한다. 다음으로, 비면허 대역 셀룰러 통신의 다음 두 가지 향상된 기능을 고려합니다. 대역 독립형 셀룰러 통신. 기존 Wi-Fi 분석 모델로는 LAA의 성능을 평가할 수 없다는 점을 감안하여 본 서신에서는 여러 경합 진화 된 NodeB로 구성된 LAA 네트워크의 성능을 분석하기위한 새로운 Markov 체인 기반 분석 모델을 제안합니다. LAA 프레임 구조 오버 헤드의 변형. LTE-LAA는 LTE에서 상속 된 속도 적응 알고리즘을 위해 적응 변조 및 코딩 (AMC) 을 채택합니다. AMC는 진화 된 nodeB (eNB)가 현재 전송의 채널 품질 표시기 피드 백을 사용하여 다음 전송을위한 변조 및 코딩 방식 (MCS)을 선택하도록 돕습니다. 라이선스 대역에서 동작하는 기존 LTE의 경우 노드 경합 문제가 없으며 AMC 성능 에 대한 연구가 잘 진행되고 있습니다. 그러나 비면허 대역에서 동작하는 LTE-LAA 의 경우 충돌 문제로 인해 AMC 성능이 제대로 처리되지 않았습니다. 이 편지에서는 AMC 운영을 고려한 현실적인 채널 모델에서 LTELAA 성능을 분석하기위한 새로 운 Markov 체인 기반 분석 모델을 제안합니다. 무선 네트워크 분석에 널리 사용되는 Rayleigh 페이딩 채널 모델을 채택하고 분석 결과를 ns-3 시뮬레이터에서 얻은 결과 와 비교합니다. 비교 결과는 평균 정확도가 99.5%로 분석 모델의 정확도를 보여줍

니다. 높은 데이터 속도에 대한 요구 사항으로 인해 3GPP는 LTE-LAA를위한 다중 반송파 운영을 제공했습니다. 그러나 다중 반송파 동작은 OOBE에 취약하고 제한된 전송 전력을 사용하여 비효율적 인 채널 사용을 초래합니다. 본 논문은 채널 효율을 높이기위한 새로운 다중 반송파 접근 방식을 제안한다. 우리가 제안한 방식은 전송 버스트를 여러 개로 분할하고 전송 전력 제한을 충족하면서 짧은 서브 프레임 전송 을 사용합니다. 또한 채널 상태를 정확하게 판단하여 OOBE 문제를 극복 할 수있는 에너지 감지 알고리즘을 제안합니다. 소프트웨어 정의 라디오를 사용하는 프로토 타입은 99% 이상의 정확도로 채널 상태를 결정하는 에너지 감지 알고리즘의 실행 가능성과 성능을 보여줍니다. ns-3 시뮬레이션을 통해 제안 된 다중 반송파 액세스 방식이 기존 LBT 유형 A 및 유형 B에 비해 사용자인지 처리량에서 각각 최대 59% 및 21.5%의 성능 향상을 달성 함을 확인했습니다. 레거시 LAA에는 배포 문제가 있기 때문에 3GPP와 MulteFire 얼라이언스는 비면허 대역 독립형 셀룰러 통신 시스 템을 제안했습니다. 그러나, 종래의 비면허 대역 독립형 셀룰러 통신 시스템은 상향 링크 제어 메시지의 전송 확률이 낮다. 이 논문은 Wi-Fi 블록 ACK 프레임에 업 링크 제어 메시지를 넣는 W ARQ : Wi-Fi 지원 HARQ를 제안합니다. 또한 W-ARQ의 처 리 성능을 향상시키기 위해 병렬 HARQ 및 클러스터링 된 Minstrel을 제안합니다. 우리가 제안한 알고리즘은 기존 MulteFire가 거의 제로 처리량 성능을 보이는 경우 높은 처리량 성능을 보여줍니다. 요약하면 비면허 대역 셀룰러 통신의 성능을 분석 합니다. 제안 된 모델을 사용함으로써 우리는 레거시 다중 반송파 동작을 주장하며 비면허 셀룰러 통신의 HARQ는 효율적이지 않다. 이러한 이유로, 우리는 최첨단 기 술에 비해 UPT 및 처리량과 같은 네트워크 성능 향상을 달성하는 OOBE 인식 추가 액세스 및 W-ARQ를 제안합니다.

감사의 글

제가 사랑하는 모든 사람들께 감사드립니다.

2021 년 2월

이재홍 올림